Estimating the power spectrum of the cosmic microwave background

J. R. Bond
Canadian Institute for Theoretical Astrophysics, Toronto, Ontario, Canada M5S 3H8

A. H. Jaffe
Center for Particle Astrophysics, 301 LeConte Hall, University of California, Berkeley, California

L. Knox
Canadian Institute for Theoretical Astrophysics, Toronto, Ontario, Canada M5S 3H8
(Received 25 August 1997; published 16 January 1998)

We develop two methods for estimating the power spectrum, C_ℓ, of the cosmic microwave background from data and apply them to the Cosmic Background Explorer Differential Microwave Radiometer and Saskatoon datasets. One method involves a direct evaluation of the likelihood function, and the other is an estimator that is a minimum-variance weighted quadratic function of the data. Applied iteratively, the quadratic estimator is not distinct from likelihood analysis, but is rather a rapid means of finding the power spectrum that maximizes the likelihood function. Our results bear this out: direct evaluation and quadratic estimation converge to the same C_ℓs. The quadratic estimator can also be used to determine directly cosmological parameters and their uncertainties. While the two methods both require $O(N^3)$ operations, the quadratic is much faster, and both are applicable to datasets with arbitrary chopping patterns and noise correlations. We also discuss approximations that may reduce it to $O(N^2)$ thus making it practical for forthcoming megapixel datasets. [S0556-2821(98)04404-X]

PACS number(s): 98.70.Vc

I. INTRODUCTION

Observations of the cosmic microwave background (CMB) anisotropy are providing strong constraints on theories of cosmological structure formation. Planned observations have the potential of providing constraints on the parameters of these theories at the percent level [1–3].

Predictions of theories for CMB anisotropy are statistical in nature. For many theories, the complete description is given by the power spectrum, C_ℓ, defined below. Thus extraction of C_ℓ from the data is of utmost importance as an end in itself and for purposes of ''radical compression'' [4,5].

With the assumption of the Gaussianity of the data, the likelihood function—the probability of the data given a particular theory—takes a simple form; with the further assumption of a prior uniform in the parameters, the likelihood is proportional to the posterior distribution of the parameters, given the data. This is precisely the quantity one wants and thus likelihood analysis has been used extensively for calculating the constraints on parameters given by CMB data. This is true whether the parameters are those of the power spectrum itself or cosmological parameters.

Another approach has been to form estimators that are quadratic functions of the data, *e.g.*, [6]. This procedure has been improved recently by the use of minimum-variance weighting of all the pairs of data points [7,8]. In this paper we present a unification of the quadratic and likelihood approaches. We show that, when used iteratively, the minimum-variance weighted quadratic estimator is a fast technique for finding the maximum of the likelihood function.

In Section II we introduce the likelihood function, explain our method for evaluating it directly, and derive the quadratic estimator. We apply quadratic estimation and direct evaluation to the case of Cosmic Background Explorer (COBE) Differential Microwave Radiometer (DMR) [9] in Section III. Both methods involve iteration and we find that for both, the iteration converges rapidly, with excellent agreement between the two methods on the final C_ℓs and their variances. However, the higher moments of the probability distribution cannot be estimated with the quadratic approach—and we find that there are significant deviations from Gaussianity in the likelihood as a function of C_ℓ. We discuss these differences, problems arising from them and possible solutions.

For COBE DMR we estimate every individual C_ℓ (for $2 \leqslant \ell \leqslant 24$) since the data allow us to determine these with some precision. The quadrupole, C_2, has received more attention in previous work than any of the other moments because of its small value and because it is the most susceptible to contamination by emission from our galaxy [10]. We also find the quadrupole to be quite small, $C_2 = 149 \pm 126\ \mu\mathrm{K}^2$, compared to $C_2 = 810\ \mu\mathrm{K}^2$ for COBE-normalized standard cold dark matter (CDM). However, due to the strong skewness of the probability distribution for C_2, 25% of the probability is actually above the COBE-normalized CDM value of C_2. Thus consistency with relatively flat models like standard CDM does not require the quadrupole power to have been reduced by systematic errors.

For most observations, which only cover a small fraction of the sky, estimating every C_ℓ is not possible. One must be content with estimating the power spectrum either with some binning in ℓ or through some other parameterization. Therefore in Section IV we discuss binning and rebinning. Then in Section V we apply the methods to estimate, from the Saska-

toon (SK) data [11], the power in ten bins from $\ell=19$ to $\ell=499$.

Power spectrum estimation can be used as a form of data compression where the estimates of C_ℓ and their covariance matrix are then used to constrain cosmological parameters. Because of the great simplifications involved in working with power spectrum estimates instead of pixelized data, this is currently the only practical procedure for using all the CMB data. Such exercises have been conducted, *e.g.*, [12–14]. In Section VI we discuss the approximations involved in such a procedure and methods for reducing the resulting inaccuracies, and in Section VII we apply these results to future balloon- and satellite-borne experiments.

Unfortunately, direct evaluation of the likelihood function is an $O(N^3)$ operation, where N is the number of data points. And it must be evaluated many times. Thus for $N \gtrsim 10{,}000$ this procedure becomes rapidly intractable on modern workstations—at least for the most straightforward implementations. Although the speed of likelihood analysis has been greatly increased by use of signal-to-noise eigenmode compression [13,15–18], this procedure still requires an $O(N^3)$ operation to be performed at least once.

Further speed is necessary if we are to be able to analyze forthcoming megapixel datasets. The quadratic estimator may offer a means of achieving this speed. We emphasize that as we have applied it here, it is still an $O(N^3)$ operation, but believe that approximations may be made in a controlled manner to reduce it to $O(N^2)$. We discuss these problems and possible solutions in Section VIII, as well as explicitly outline our algorithm for power spectrum estimation from CMB data.

II. METHODS: LIKELIHOOD ANALYSIS

We begin by establishing the notation used for describing the pixelized data of a CMB observation. We also define the power spectrum, C_ℓ, and the likelihood function. With this common groundwork complete, we then move on to a description of the two different methods for estimating C_ℓ.

A. The likelihood function

In general, CMB observations are reduced to a set of binned observations of the sky, or pixels, Δ_i, $i=1,\ldots,N$ together with a noise covariance matrix, $C_{nii'}$. We model the observations as contributions from signal and noise:

$$\Delta_i = s_i + n_i . \tag{2.1}$$

We assume that the signal and noise are independent with zero mean, with correlation matrices given by

$$C_{Tii'} = \langle s_i s_{i'} \rangle ; \quad C_{nii'} = \langle n_i n_{i'} \rangle \tag{2.2}$$

so

$$\langle \Delta_i \Delta_{i'} \rangle = C_{Tii'} + C_{nii'} \tag{2.3}$$

where $\langle \ldots \rangle$ indicate an ensemble average. With the further assumption that the data are Gaussian, these two point functions are all that is necessary for a complete statistical description of the data.

One important complication to the above description comes from the existence of constraints. Often the data, Δ_i, are susceptible to a large source of noise, or a not-well-understood source of noise that contaminates only one mode of the data. For example, the average value of Δ_i may be very poorly determined. In this case, the average is usually subtracted from Δ_i. Similarly, the monopole and dipole are explicitly subtracted from the all-sky COBE DMR data, because the monopole is not determined by the data and the dipole is local in origin. In general, placing any constraint on the data or some subset thereof, such as insisting that its average be zero, results in additional correlations in Δ_i. We take this into account by adding these additional correlations, C_C, to the noise matrix to create a ''generalized noise matrix,'' C_N, where $C_N = C_n + C_C$. In the limit that the amplitude of C_C gets large, this is equivalent to projecting out those modes which are now unconstrained by the data [19], but this scheme is numerically much simpler to implement. Thus in the text below, we always write the noise matrix as C_N instead of C_n. The details of this procedure for handling the effect of constraints are explained in Appendix A.

Due to finite angular resolution and switching strategies designed to minimize contributions from spurious signals (such as from the atmosphere), the signal is generally not simply the temperature of the sky in some direction, $T(\hat{x})$, but a linear combination of temperatures:

$$s_i = \int d\Omega H(\hat{x},\hat{x}_i) T(\hat{x}) \tag{2.4}$$

where $H(\hat{x},\hat{x}_i)$ is sometimes called the ''beam map,'' ''antenna pattern'' or ''synthesis vector.'' If we discretize the temperature on the sky, then we can write the beam map in matrix form, $s_i = \Sigma_n H_{in} T_n$.

The temperature on the sky, like any scalar field on a sphere, can be decomposed into spherical harmonics

$$T(\theta,\phi) = \sum_{\ell m} a_{\ell m} Y_{\ell m}(\theta,\phi). \tag{2.5}$$

If the anisotropy is *statistically* isotropic, *i.e.*, there are no special directions in the mean, then the variance of the multipole moments, $a_{\ell m}$, is independent of m and we can write:

$$\langle a_{\ell m} a^*_{\ell' m'} \rangle = C_\ell \delta_{\ell\ell'} \delta_{mm'}. \tag{2.6}$$

For theories with statistically isotropic Gaussian initial conditions, the angular power spectrum, C_ℓ, is the entire statistical content of the theory in the sense that any possible predictions of the theory for the temperature of the microwave sky can be derived from it.[1] Even for non-Gaussian theories, the angular power spectrum is a very important statistic, probably the most important one for determining the viability of the most popular non-Gaussian theories. However, the techniques we present in this paper for estimating the power spectrum assume that the fluctuations in both the sky signal and experimental noise are Gaussian.

The theoretical covariance matrix, $C_{Tii'}$, is related to the angular power spectrum by

[1]Non-linear evolution will produce non-Gaussianity from Gaussian initial conditions, but this is quite sub-dominant for $\ell \lesssim 1000$.

$$C_{Tii'} = \sum_{\ell} \frac{2\ell+1}{4\pi} C_\ell W_{ii'}(\ell) \ , \tag{2.7}$$

where

$$W_{ii'}(\ell) = \sum_{nn'} H_{in} H_{i'n'} P_\ell(\cos\theta_{nn'}) \tag{2.8}$$

is called the window function of the observations and $\theta_{nn'}$ is the angular separation between the points on the sphere labeled by n and n'.

Let us define the quantity $\mathcal{C}_\ell \equiv \ell(\ell+1)C_\ell/(2\pi)$. This is useful for two reasons: it is the logarithmic average of $\mathcal{C}_\ell$ that gives the variance of the data and (therefore) for scale-invariant theories of structure formation, $\mathcal{C}_\ell$ is roughly constant at large scales.

Within the context of a model, the $\mathcal{C}_\ell$ depend on some parameters, a_p, $p=1,\ldots,N_p$ which could be the Hubble constant, baryon density, redshift of reionization, etc. The theoretical covariance matrix will depend on these parameters through its dependence on $\mathcal{C}_\ell$. We can now write down the likelihood function for a_p, which is equal to the probability of the data given a_p:

$$\mathcal{L}_\Delta(a_p) = P(\Delta|a_p) = \frac{1}{(2\pi)^{N/2}|C_T(a_p)+C_N|^{1/2}} \times \exp\left[-\frac{1}{2}\Delta^T[C_T(a_p)+C_N]^{-1}\Delta\right]. \tag{2.9}$$

One can then search for the parameters a_p that maximize this likelihood.

B. Direct evaluation of the likelihood function

First, we must choose a set of parameters to characterize the theoretical covariance, C_T. For a given class of cosmological theories (*e.g.*, adiabatic perturbations from inflation), we can calculate the power spectrum from some set of parameters like the densities of various components, Ω_x, the shape of the primordial power spectrum, the Hubble constant, etc. A detailed exploration of the cosmological parameter space constrained by current CMB and large-scale structure data is given in [13]. Alternately, we can describe the power spectrum by its actual value at some discrete multipoles or bands of ℓ. Moreover, all of the information in the experiment (again, for Gaussian theories) is captured in the likelihood function for the power spectrum:

$$P(\Delta|\{a_p\}) \propto P(\Delta|\{C_\ell(a_p)\}). \tag{2.10}$$

In this paper, we concentrate on the $\mathcal{C}_l$ parameterization in order to determine the power spectrum directly from the data. In principle, we would like to calculate the full likelihood as a function of the power spectrum $P(\Delta|\{C_\ell\})$ for some $\ell \leqslant \ell_{\rm max}$; at the very least we would like to find the maximum of this $\ell_{\rm max}$-dimensional function, and its properties (*e.g.*, curvature or ''width'') around this maximum.

Searching such multi-dimensional spaces can be difficult; in this case, each evaluation of the likelihood function is an expensive $O(N^3)$ matrix manipulation and a brute force search through the parameter space would take of order $(\mathcal{C}_\ell/\delta\mathcal{C}_\ell)^{\ell_{\rm max}}$ such evaluations to reach an accuracy of $\delta\mathcal{C}_\ell$. In our applications, we have found that the space is sufficiently structureless that a simple iteration procedure works well for finding the maximum. In addition, we do not use all of the individual C_ℓ values as separate parameters, since experiments do not have uncorrelated information about bands of width $\Delta\ell \lesssim 2\pi/\theta$, where θ is the angular extent of the survey [20]. For COBE DMR, we bin in bands of width $\Delta\ell = 2-3$ for $\ell \geqslant 25$ and only consider $\ell \leqslant 35$; above this multipole we give the power spectrum a constant shape and amplitude (that of COBE-normalized standard CDM, in this case). For SK, we have tried bins of various widths, the choice of which we will discuss below.

At the first iteration, we choose some appropriate starting $\mathcal{C}_\ell$. For each ℓ (or band), we hold all other $\mathcal{C}_\ell$s fixed, while the one of interest is allowed to vary; in the appropriate signal-to-noise basis, the likelihood as a function of this single parameter is trivial to compute (see Appendix A). That is, for each band labeled by B, we rewrite the correlation matrix as

$$C_T + C_N = q_B C_B + C_{N*} \tag{2.11}$$

(no sum over B), where the effective signal and noise matrices are given by

$$C_{Bii'} = \sum_{\ell \in \rm B} \frac{2\ell+1}{4\pi} C_\ell W_{ii'}(\ell);$$

$$C_{N*ii'} = C_{Nii'} + \sum_{L \notin \rm B} \frac{2L+1}{4\pi} C_L W_{ii'}(L) \tag{2.12}$$

and calculate the likelihood as a function of the adjustment factor q_B alone. After going through all the ℓ bands of interest, we then update the starting power spectrum by multiplying the C_ℓs in each band by the q_B that maximized the likelihood function. We then repeat. Convergence is achieved when all the q_Bs equal unity. For COBE DMR, starting from COBE-normalized standard CDM (already a good fit), we achieved convergence at the few percent level after only two such iterations for $\ell \leqslant 20$; after 10 iterations, convergence is everywhere better than 10^{-4}.

There is a drawback to the procedure as described so far, compared to what could be achieved by more ambitious methods such as simulated annealing [21,1]. Even though we find the maximum of the likelihood function, we have not accurately determined its shape—only the shape along each $\mathcal{C}_\ell$, while the others are held constant (*i.e.*, parallel to the axes of the $\ell_{\rm max}$-dimensional space). And we have no estimate for the correlations between the uncertainties in each estimate of $\mathcal{C}_\ell$. Below, we shall see how to use the Fisher matrix for an estimate of these correlations. Clearly, a more ambitious minimization strategy would be preferable; we have chosen not to implement one since the quadratic estimator to be derived below achieves this end without any explicit likelihood calculation.

We have also considered the possibility of estimating each $\mathcal{C}_\ell$ assuming no other knowledge of all of the others. That is, we have attempted to marginalize over the $\mathcal{C}_\ell$ values

outside of each band. This is equivalent to the procedure outlined in Appendix A for marginalizing over removed constraints (averages, dipoles, etc.) and foreground templates. However, in this case, the method fails to constrain the power spectrum. In performing this marginalization, we effectively allow an arbitrary amount of noise consistent with *any power spectrum at all* outside of the band of interest. That is, we multiply the second term in Eq. (2.12) by a very large number to make the variance in those modes larger than the noise or (expected) signal. For a perfect, all-sky observation, this would not be a hindrance since all the multipoles are independent. For any realistic observation, however, there is aliasing of different multipoles together; some modes of the data (defined, for example, by the eigenmodes of Appendix A) that are being marginalized over will have nonzero contributions from within the $\not\ell$-band of interest. Thus, the new *noise* spectrum alone will span the space of possible *signals*, consistent with having no power at all in the band. This just reinforces the idea that any unknown noise in the observation should ideally be completely ''orthogonal'' to the quantities we are attempting to estimate (which will often be the case when the marginalization technique is used for experimental constraints or foreground removal).

C. Gaussian approximation to the likelihood function

If the likelihood function is continous and has a peak then it can be approximated as a Gaussian near the peak. For well-constrained parameters this approximation should be good except in the tails of the distribution. A Gaussian approximation to the likelihood function can be obtained by truncating the Taylor expansion of $\ln\mathcal{L}$ about a_p at second order in δa_p:

$$\ln\mathcal{L}(a+\delta a)=\ln\mathcal{L}(a)+\sum_p \frac{\partial\ln\mathcal{L}(a)}{\partial a_p}\delta a_p + \frac{1}{2}\sum_{pp'} \frac{\partial^2\ln\mathcal{L}(a)}{\partial a_p\partial a_{p'}}\delta a_p\delta a_{p'}. \quad (2.13)$$

This Gaussian approximation is useful because now, instead of making multiple evaluations of the likelihood function, we can directly solve for the δa_p that maximize it:

$$\delta a_p=-\sum_{p'}\left(\frac{\partial^2\ln\mathcal{L}(a)}{\partial a_p\partial a_{p'}}\right)^{-1}\frac{\partial\ln\mathcal{L}(a)}{\partial a_{p'}}. \quad (2.14)$$

The first derivative is given by

$$\frac{\partial\ln\mathcal{L}(a)}{\partial a_{p'}}=\frac{1}{2}\mathrm{Tr}[(\Delta\Delta^T-C)(C^{-1}C_{T,p'}C^{-1})] \quad (2.15)$$

and the second derivative by

$$\mathcal{F}^{(a)}_{pp'}\equiv-\frac{\partial^2\ln\mathcal{L}(a)}{\partial a_p\partial a_{p'}}=\mathrm{Tr}\left[(\Delta\Delta^T-C)\left(C^{-1}C_{T,p}C^{-1}C_{T,p'}C^{-1} - \frac{1}{2}C^{-1}C_{T,pp'}C^{-1}\right)\right]+\frac{1}{2}\mathrm{Tr}(C^{-1}C_{T,p}C^{-1}C_{T,p'}) \quad (2.16)$$

where Tr is the trace, $C\equiv C_T+C_N$ is the total covariance matrix and $_{,p}\equiv\partial/\partial a_p$. We call the second derivative the curvature matrix and give it the symbol $\mathcal{F}^{(a)}$, where the (a) indicates that we have taken the derivative of $\ln\mathcal{L}$ with respect to a.

To the extent that the likelihood function is not Gaussian, we will not have correctly solved for its maximum. Thus we iterate. The closer we get to the maximum, the better the quadratic approximation to $\ln\mathcal{L}$ will become. This is exactly the Newton-Raphson method for finding the zero of $\partial\ln\mathcal{L}/\partial a_p$. The procedure is not fool-proof—there is the risk of getting trapped in a local extremum. In practice we have found the likelihood function to be sufficiently structureless that this is not a problem.

D. Quadratic estimator

The above procedure is not exactly what we do in practice. Calculating the curvature matrix is a computationally intensive procedure. Matters simplify significantly if we settle for the ensemble average quantity, called the Fisher matrix, F:

$$F^{(a)}_{pp'}\equiv\langle\mathcal{F}^{(a)}_{pp'}\rangle = \frac{1}{2}\mathrm{Tr}(C^{-1}C_{T,p}C^{-1}C_{T,p'}). \quad (2.17)$$

When taking this ensemble average, denoted by $\langle\ldots\rangle$, we assume that the theory is correct and therefore that $\langle\Delta\Delta^T\rangle=C$.

Note that the Fisher matrix, like the curvature matrix, is defined with respect to particular parameter choices. If we transform to a new set of parameters, $\tilde{a}_p$ then the Fisher matrix for these new parameters is $F^{(\tilde{a})}=Z^{-1}F^{(a)}(Z^{-1})^T$, where $Z_{pp'}=\partial\tilde{a}_p/\partial a_{p'}$. Tegmark offers a proof of this [7]; with our approach it is obvious from the definition of the curvature matrix in Eq. (2.16).

Replacing the curvature matrix with the Fisher matrix makes our estimator for a_p quadratic in the data, Δ:

$$\delta a_p=\frac{1}{2}\Sigma_{p'}(F^{(a)})^{-1}_{pp'}\mathrm{Tr}[(\Delta\Delta^T-C)(C^{-1}C_{T,p'}C^{-1})]. \quad (2.18)$$

This is what we call the quadratic estimator. The right-hand side depends on a_p, so we pick an initial a_p, calculate the correction δa_p, and then repeat for the new value of a_p. Note that the power spectrum estimate is not constrained to be positive-definite—a point we discuss below.

If we assume that the input theory is correct, then $\langle\Delta\Delta^T\rangle=C$ and therefore Eq. (2.18) implies $\langle\delta a_p\rangle=0$. Similarly, one can work out that $\langle\delta a_p\delta a_{p'}\rangle=(F^{(a)})^{-1}_{pp'}$. This is to be expected since for a Gaussian distribution, the two-point function is the inverse of the curvature matrix.

Although the quadratic involves using the Fisher matrix F as an approximation to the full curvature matrix $\mathcal{F}$, both procedures iterate to the *same* parameters, the maximum of the likelihood function. This is because both $\mathcal{F}$ and F are invertible, so $\delta a_p=0$ from either procedure implies $\partial\ln\mathcal{L}/\partial a_p=0$. Thus, when applied iteratively, *the quadratic*

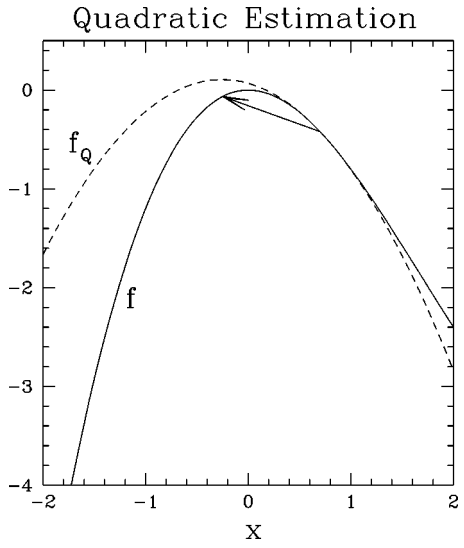

FIG. 1. A one-dimensional example of quadratic estimation.

estimator will find the exact location of the likelihood peak; the only approximation comes in using the Fisher matrix to approximate the errors, rather than the full curvature matrix (and below we show that in the cases studied, this is a very good approximation; moreover, having found the location of the peak, the curvature there can be calculated explicitly if necessary).

Our procedure is very similar to that of the Levenberg-Marquardt method [21] for minimizing a χ^2 with non-linear parameter dependence. There the curvature matrix (second derivative of the χ^2) is replaced by its expectation value and then scaled according to whether the χ^2 is reduced or increased from the previous iteration. Similar manipulations of the Fisher matrix may possibly speed convergence of the likelihood maximization, although one would want to do this without direct evaluation of the likelihood function.

In our applications to COBE DMR and SK we have found that iteration converges quickly. Iteration is especially important for the calculation of the error covariance matrix. Without iteration, the errors are determined entirely by the initial theoretical assumptions and are not influenced by the data. (Of course, this is exactly why the Fisher matrix has been so useful in determining how well future observations will be able to determine parameters.)

As we have defined it so far, the quadratic estimator with the iteration procedure is a method for finding the maximum of the likelihood. Only if one takes the prior probability to be uniform in the parameters is this equivalent to maximizing the posterior probability. We could, of course, include different priors directly in the definition of the estimator. The derivation would then begin by changing Eq. (2.13) to a Taylor expansion of $\ln P_{\rm post}$ where $P_{\rm post} \propto \mathcal{L} P_{\rm prior}$ is the posterior probability distribution and $P_{\rm prior}$ is the (differentiable) prior distribution.

To see how the quadratic estimator works, we can take a one-dimensional example (see Fig. 1). Consider a function f, that is approximately quadratic. If we take its first and second derivatives about some point, x_0 ($=0.7$ in the figure), we can construct the function f_Q which approximates f. By finding the value of x that maximizes f_Q, we have a guess as to the maximum of f. Now, for a further refinement of the estimate, a new f_Q can be calculated based upon the properties of f at this new value of x. (Note that the full quadratic estimator of Eq. (2.18) includes the further approximation of using the Fisher matrix [Eq. (2.17)] rather than the actual curvature matrix [Eq. (2.16)] for the second derivative of the log-likelihood.)

The applications we discuss in the following all use the $\mathcal{C}_\ell$s as the parameters a_p. In this case,

$$C_{Tii',\ell} \equiv \frac{\partial C_T}{\partial \mathcal{C}_\ell} = \frac{\ell + 1/2}{\ell(\ell+1)} W_{ii'}(\ell) \simeq W_{ii'}(\ell)/\ell . \tag{2.19}$$

We also consider the power spectrum averaged over some bands B with some assumed shape $\mathcal{C}_\ell^{\rm shape}$; in that case, we average the above weighted by the shape:

$$C_{Tii',B} = \sum_{\ell \in B} C_{Tii',\ell} \mathcal{C}_\ell^{\rm shape} . \tag{2.20}$$

However, there is also the interesting possibility of taking the a_p as the cosmological parameters that affect the spectrum, Ω, h, n_S, Ω_b, etc. Iteration in this case should also converge to the likelihood maximum.

We note that the quadratic estimator discussed here can also be derived by finding the quadratic function of the data that is unbiased and has minimum variance. For a full discussion of the quadratic in this context, see [7,22,23]. The quadratic function of the data derived this way is the same as Eq. (2.18). However, the estimate is only unbiased if there is no iteration. Since the end point of (successful) iteration is the maximum likelihood, the iterated estimator is, like all maximum likelihood estimators, only asymptotically unbiased.

The methods we have used can also be applied to optimal determination of the correlation function in angular bins. The optimal signal plus noise weighting suggested for correlation function determination differs from the usual diag$[C_n^{-1}]$ weighting applied to COBE DMR.

E. Single bandpower estimation

It has now become conventional to characterize switching experiments which covered small patches of the sky by a single bandpower [15], placing the estimated power at a location related to the window function of the experiment. In this case, there is just one parameter to determine. The quadratic statistic reduces to

$$Q_B = \frac{\Delta^\dagger C^{-1} C_T C^{-1} \Delta - {\rm Tr}\, C_N C^{-1} C_T C^{-1}}{{\rm Tr}\, C_T C^{-1} C_T C^{-1}} . \tag{2.21}$$

If the optimal weight C^{-1} is replaced by the diagonal part of C_n^{-1}, then this is related to the quadratic statistic proposed by Boughn and Cottingham [24], which has been applied to the COBE DMR and Far Infrared Survey (FIRS) is unbiased and has data using Monte Carlo simulations to define its distribution. With the optimal weighting and the proper inclusion of constraints in C_N, the values of Q_B and its error estimation are of direct use. As discussed above, the iterated quadratic estimator for the amplitude will converge to the maximum likelihood value. The parameter

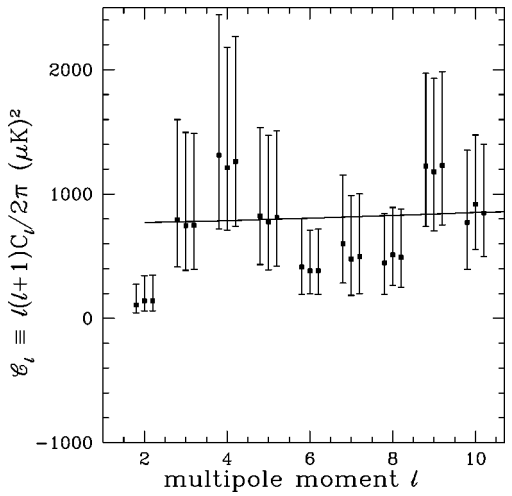

FIG. 2. Maximum-likelihood power spectra from iterative direct evaluation of the likelihood function. The curve is the zeroth iteration: COBE-normalized standard CDM. The points with error bars are, from left to right, the results of the first to third iterations. Here, we define the error bars by a likelihood ratio of $e^{-1/2}$ from the peak.

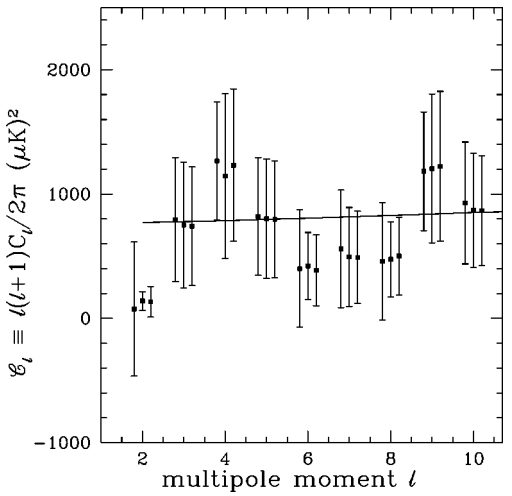

FIG. 3. Iterative quadratic estimation. The curve is the zeroth iteration: COBE-normalized standard CDM. The points with error bars are, from left to right, the results of the first to third iterations.

Q_B could be any squared amplitude characterizing the assumed theoretical $\mathcal{C}_\ell$, such as the σ_8^2 used to characterize the strength of the power spectrum on cluster scales. To translate to an average bandpower one must evaluate $Q_B\langle \mathcal{C}^{\rm shape}{}_\ell\rangle_B$, using an appropriately weighted average of $\mathcal{C}^{\rm shape}{}_\ell$ over the single band B. Issues associated with such averaging are addressed in Section IV. Current and future experiments cover large enough patches of the sky that characterizing their results by single bandpowers is not useful, but evaluation of power spectrum normalization amplitudes (such as σ_8) for particular theories will always be of use.

III. APPLICATION TO COBE DMR

We first apply these methods to the anisotropy measurements of the COBE DMR instrument [9,25]. The DMR instrument actually measured a complicated set of temperature differences 60° apart on the sky, but the data were reported in the much simpler form of a temperature map, along with appropriate errors (which we have expanded to take into account correlations generated by the differencing strategy, as treated in [16], following [26]). The calculation of the theoretical correlation matrix includes the effects of the beam, digitization of the time stream, and an isotropized treatment of pixelization, using the table given by Kneissl and Smoot [27], modified for resolution 5. We use a weighted combination of the 31, 53 and 90 GHz maps. Because most of the information in the data is at large angular scales, we use the maps degraded to ''resolution 5'' which has 1536 pixels. Further, we cannot of course observe the entire CMB sky; we use the most recent galactic cut suggested by the DMR team [9], leaving us with 999 pixels to analyze. We use the galactic, as opposed to ecliptic, pixelization.

For both methods we iterated 28 parameters: $\mathcal{C}_2$ to $\mathcal{C}_{24}$ individually, $\mathcal{C}_{25}$ to $\mathcal{C}_{32}$ grouped into bins of width 2 and finally $\mathcal{C}_{33}$ through $\mathcal{C}_{35}$ grouped into one bin. Binning is described in more detail prior to the Saskatoon application where it is much more important.

In Figs. 2 and 3 we see the results of the iterative procedures described in the previous section. Figure 2 shows the results of direct evaluation and Fig. 3 shows the results of quadratic estimation. Moments $\ell > 10$ are not shown to avoid clutter. From left to right are the first to third iterations, together with their error bars. The solid line is the starting point we chose, the power spectrum for COBE-normalized standard CDM. For this method, we define the estimated $\mathcal{C}_\ell$ as the maximum of the likelihood function, and the errors by the value of $\mathcal{C}_\ell$ where the likelihood drops by a factor $e^{-1/2}$ from that maximum.

First we will discuss the direct evaluation method. The iteration converges rapidly. The maximum likelihood values of a fourth iteration (shown in Fig. 4) typically differ from the third by 1–3% of the error bars (for $2 \leqslant \ell \leqslant 19$) with a maximum deviation of 7% at $\ell = 12$. In the limit that the moments were independent, there would be no need for iteration; iteration is only necessary because of the influence

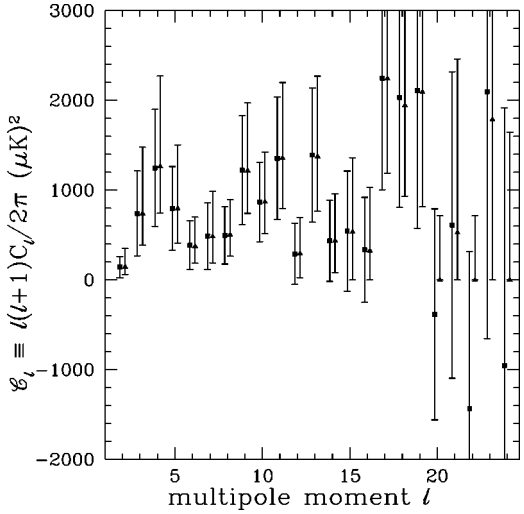

FIG. 4. We compare the results of the quadratic and direct evaluation iteration schemes. At each ℓ, the left error bar (square symbol) is for the quadratic, the right (triangle) is for the direct evaluation.

that the value of one band has on the best value of another. The rapidity of the convergence is expected because, as we will see below, the moments are in fact fairly uncorrelated. We remind the reader that the error bars given by this method—indeed the whole probability distribution for each $\mathcal{C}_\ell$—are calculated by holding the others fixed.

Iteration is also quite rapid for the quadratic estimator: the maximum likelihood values of a fourth iteration (shown in Fig. 4) differ from the third by better than 1% of the square root of the variance for $\ell \leqslant 24$, except for the quadrupole and $\ell = 20$ which are slightly worse, converging to 3%. Just like the direct method, most of the change in the maximum likelihood estimate occurs in the first iteration.

Unlike the direct method, the error bars of the first iteration are quite different from the error bars of the later iterations. That is because the error bars (the Fisher matrix) do not depend on the data, but only on the input power spectrum. Therefore the data have had no effect on the error bars until the second iteration is reached. To the extent that the distribution is Gaussian, these error bars accurately represent the uncertainty on each parameter; they take into account the correlations with the other parameters. The largest changes in the error bars from 1st to 2nd, 2nd to 3rd and 3rd to 4th are 610% ($\ell = 2$), 60% ($\ell = 2$) and 6.5% ($\ell = 6$), respectively. From the 3rd to the 4th, most of the changes are less than 1%.

In the previous section it was claimed that the curvature matrix is a good approximation to the Fisher matrix. We have explicitly checked this for the final iteration and find that for $\ell < 20$ most of the Fisher matrix and curvature matrix derived error bars agree with each other to better than 4%. The worst cases are $\ell = 4$ and $\ell = 5$ at 13% and 15%.

Not only do these methods converge, but they converge to the same power spectrum, as we see in Fig. 4. The differences between the final iterations are less than 2% of the quadratic error bars for $\ell < 20$, except for a 4% difference at $\ell = 18$; at higher moments, the methods often do not detect positive power. Note that at multipoles where both methods do detect nonzero power, the quadratic method gives error bars which are systematically smaller (than those of the direct method) in the direction of positive power, and systematically larger towards lower power. This can be understood as a result of the considerable non-Gaussian skewness of the distribution of power, as seen in Fig. 5. Also note that when the likelihood maximum is at zero power, the quadratic estimate is at (physically meaningless) negative power. This is to be expected since the existence of a maximum at $\mathcal{C}_\ell = 0$ implies $\partial \ln \mathcal{L} / \partial \mathcal{C}_\ell \leqslant 0$, and therefore the Gaussian fit to $\ln \mathcal{L}$ at $\mathcal{C}_\ell = 0$ will peak at $\mathcal{C}_\ell \leqslant 0$.

We have also checked that using the full resolution 6 data (3881 pixels after the galactic cut) changes the results of the maximum-likelihood estimate for the power spectrum by much less than one sigma. We have checked in detail using the direct evaluation, for which the resolution 6 results differ from those at resolution 5 by less than 5% for $\ell \leqslant 15$, except at $\ell = 6-9$ where the difference is almost 10–20% and at $\ell = 12$ and $\ell = 14$, where the difference is nearly 50%, still smaller than the large error at these ℓ; the higher resolution data give an overall normalization that differs by 4% (compared with an error of 14%) from that of the best quadratic computed at resolution 5. These differences are consistent

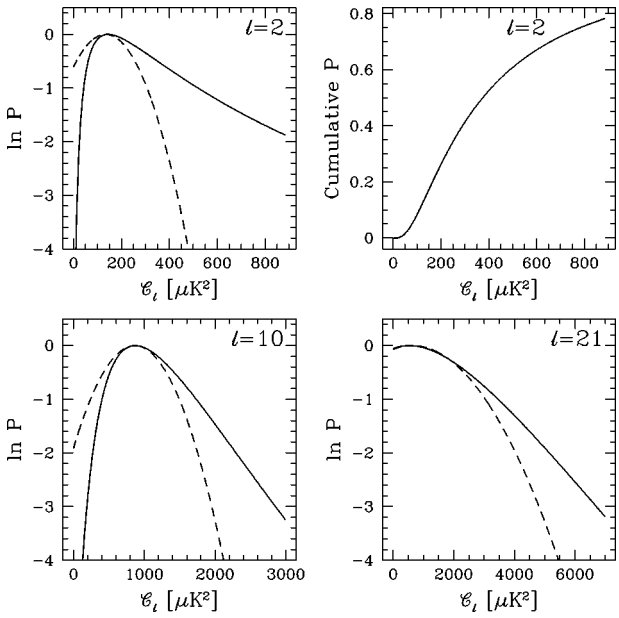

FIG. 5. Probability distributions for individual $\mathcal{C}_\ell$ values, as labeled, for a prior uniform in $\mathcal{C}_\ell$. The solid curve is the true likelihood from the last iteration of the full evaluation; the dotted curve is the Gaussian approximation from the last iteration of the quadratic procedure. For $\ell = 2$, we also show the cumulative probability distribution, properly normalized to unit probability as $\mathcal{C}_\ell \to \infty$.

with those observed for different pixelizations and galactic cuts [9,25]; note that both the direct evaluation and quadratic procedures converge with considerably higher precision than these intrinsic errors, even for $\ell \gtrsim 15$ where the pixelization differences become important and, simultaneously, the noise begins to dominate.

We also agree at least qualitatively with other calculations that we have compared to, in all cases (with detected power) well within the various reported error bars. In Fig. 6 we show a comparison of our quadratic results with those of [17,25], both of whom use a maximum likelihood method. Gorski

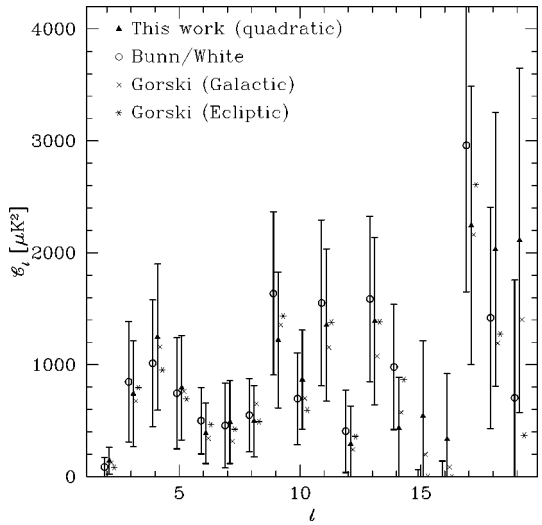

FIG. 6. Comparison of different groups' power spectrum estimates, as marked. Gorski computes power spectra in both ecliptic and galactic pixelizations of the sky.

[25] uses a complete search through parameter space with ''cut-sky spherical harmonics'' to speed up the calculation; Bunn and White [17] also use the signal-to-noise transformation of Appendix A to increase speed. The results of our first quadratic iteration also have qualitative agreement with Tegmark's implementation of the quadratic estimator [7].

The fact that three completely different methods achieve similar results lends support to the claim that the final estimates are unaffected by the choice of initial starting place, and the stronger claim that they would have resulted from *any* starting place. From the Fisher matrix and from the probability distributions of Fig. 5 it should be evident that this likelihood space is fairly structureless. We could have started anywhere and converged to the same place, although perhaps slightly less rapidly. We note though that if the correlations were stronger between the different $\mathcal{C}_\ell$s, the direct method would be less robust. In particular, if the initial power spectrum were much too large, then each multipole moment would try to make up for this all by itself by coming out very small. Thus there could be large oscillations—conceivably without convergence. In addition, these correlations, combined with the width of the likelihood function, imply that our iterative direct evaluation method for finding the peak may not converge to a unique maximum, as values oscillate between iterations; in practice, we have found that the changes remain much smaller than the size of the error bars, as noted above. Such a broad likelihood function indicates that the data do not strongly prefer a unique maximum. Nonetheless, if we desire to find the exact location of the peak, a more complete search through the many-parameter space (as in [17,25]) or the use of the quadratic method will be necessary.

The probability distributions of the parameters are different for the two different methods because of the approximation of independence by the direct method and the approximation of Gaussianity by the quadratic method. We can see those differences in Fig. 5. The departure from Gaussianity is most dramatic for the quadrupole. According to the Gaussian distributions of $\mathcal{C}_2$, COBE-normalized CDM with $\mathcal{C}_2 = 770\ \mu\mathrm{K}^2$ is over five standard deviations away from the mean, highly ruled out. But the strong skewness of the exact likelihood function has 25% of the probability for $\mathcal{C}_2$ above $770\ \mu\mathrm{K}^2$. This is more probability than there is above only 1σ for a Gaussian distribution.[2] As ℓ increases the distributions become more Gaussian. The distribution for $\ell = 21$ is well approximated by a Gaussian as expected from the central limit theorem since there are approximately 30 independent modes of roughly equal weight contributing to the constraint.

The highly non-Gaussian nature of some of these distributions implies that other definitions of the point estimation and the error bars are possible. First, we could consider the mean or median of the distribution, rather than its maximum, and define errors by the amount of enclosed probability. Second, we could also have used different prior probabilities for the $\mathcal{C}_\ell$. Throughout the paper, we use a prior uniform in $\mathcal{C}_\ell$, equivalent to equating the posterior distribution with the likelihood itself. When the data constrain the power strongly (*i.e.*, small error bars), the result is insensitive to the choice of the prior; in other regimes, such as the quadrupole, $\mathcal{C}_2$, the prior has more significance. To investigate this, we have also tried other possible prior distributions, along with the definition of the point estimate by the median of the distribution. A prior $\mathrm{P}(\mathcal{C}_\ell)d\mathcal{C}_\ell \propto d\mathcal{C}_\ell/\sqrt{\mathcal{C}_\ell}$ [which is equivalent to a prior uniform in $\sigma_{\mathrm{th}} = (\mathcal{C}_\ell)^{1/2}$] gives a median $\mathcal{C}_2$ 60% higher than the likelihood maximum; the highly skewed distribution means that for a constant prior the median is 166% higher, while a prior uniform in $\ln\mathcal{C}_2$ has a median only 5% higher. Finally, we have also tried a ''Fisher Prior,'' which uses the element of the Fisher matrix [Eq. (2.17)] corresponding to $a_p = \sigma_{\mathrm{th}}$ to determine the expected amplitude,

$$P(\sigma_{\mathrm{th}}^2) \propto F_{\sigma\sigma}^{1/2} \propto \left[\mathrm{Tr}\left(\frac{\partial \ln(C_N + \sigma_{\mathrm{th}}^2 C_T)}{\partial \sigma_{\mathrm{th}}^2} \right)^2 \right]^{1/2} \qquad (3.1)$$

which is uniform in $\mathcal{C}_\ell \propto \sigma_{\mathrm{th}}^2$ at low amplitudes, but uniform in $\ln\mathcal{C}_\ell$ at high amplitudes, where the smooth transition is determined by the scale at which signal-to-noise becomes about one. For this prior, the median is about 20% higher than the maximum likelihood.

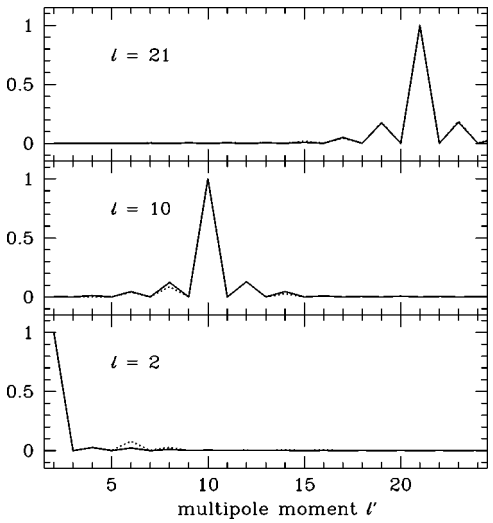

FIG. 7. Rows of the normalized DMR Fisher matrix (see text), at $\ell = 2,10,21$. The solid lines show the matrix at the zeroth iteration; the dashed lines for the final iteration.

In Fig. 7 we show the normalized Fisher matrix, $F^{(\mathcal{C})}_{\ell\ell'}/\sqrt{F^{(\mathcal{C})}_{\ell\ell} F^{(\mathcal{C})}_{\ell'\ell'}}$ to indicate the level of correlations between the different $\mathcal{C}_\ell$s. The off-diagonal terms are due to the inhomogeneous coverage, the most drastic component of which is due to the galactic cut. This cut discards all map pixels with galactic latitude $|b| \leq 20°$, with some modifications motivated by the Diffuse Infrared Background Explorer (DIRBE) dust map [9]. A map with a $|b| \leq 20°$ cut and otherwise homogeneous coverage would result in zero overlap between $Y_{\ell m}$s with opposite parity which explains the near zero values of the Fisher matrix for $\ell' - \ell$ odd [17]. Modes with similar parity do mix and hence the nonzero elements at $\ell' = \ell \pm 2$. Even these off-diagonal terms though are much smaller than the diagonal, especially for the lower multipole

[2]Also these quadrupole probability distributions do not take into account the possibility of foreground contamination. The DMR team [10] has carefully analyzed the foreground contamination and report $\mathcal{C}_2 = (273 \pm 185 \pm 360)\ \mu\mathrm{K}^2$ with statistical and systematic errors.

moments which are determined by modes with higher signal-to-noise. Iteration does not have much effect on the normalized Fisher matrix; the off-diagonal components are largely a result of the coverage geometry.

IV. METHODS: BINNING AND REBINNING

For the same reason that limited extent in the time domain leads to limited spectral resolution in the frequency domain, uncertainties in $\mathcal{C}_\ell$ and $\mathcal{C}_{\ell'}$ are strongly correlated when $\ell \lesssim 2\pi/\theta$, where θ is the linear extent of the observed region [20]. Thus binning moments together in bins of width $\Delta\ell \simeq \pi/\theta$ is a sensible thing to do. Because of the experimental noise, final bins may need to be even coarser to prevent the error bars from being excessively large.

We view binning as a two-step procedure: an initial fine binning followed by a rebinning to coarser bins. The reason for the first step is that we want to know, within each coarser bin, where the constraining information is. The finer binning gives us this knowledge. For pedagogical reasons, we start with a discussion of rebinning and then discuss the initial binning.

A. Rebinning

We assume here that the initial binning is the finest possible, $\Delta\ell = 1$, since this makes for the simplest exposition. It is easily generalized to arbitrary initial binning. For reasons that will become clear later, we begin our discussion of this rebinning procedure by reparameterizing the power spectrum in terms of an assumed spectral shape, $\mathcal{C}_\ell^{\rm shape}$. Thus the parameters we are trying to estimate are no longer $\mathcal{C}_\ell$ directly, but the deviation from the assumed shape, given by q_ℓ:

$$\mathcal{C}_\ell = q_\ell \mathcal{C}_\ell^{\rm shape}. \tag{4.1}$$

If our estimates of individual q_ℓ are too noisy, then we can average them together into coarser bins, which we will label by the subscript B. We wish to do this in a ''minimum variance'' manner. That is, we want to find Q_B that minimizes

$$\chi^2 = \sum_{\ell\ell'} (Q_B - q_\ell) F^{(q)}_{\ell\ell'} (Q_B - q_{\ell'}) \tag{4.2}$$

where the sum (like all sums in this subsection) extends over the width of the new and coarser bin. The Fisher matrix appears here because, in the Gaussian approximation to the likelihood function, the Fisher matrix is the inverse of the parameter covariance matrix. Complications due to non-Gaussianity are discussed in Section VI.

It is easy to show that the solution to this minimization problem is given by

$$Q_B = \frac{\sum_{\ell\ell'} q_\ell F^{(q)}_{\ell\ell'}}{\sum_{\ell\ell'} F^{(q)}_{\ell\ell'}}. \tag{4.3}$$

The new parameters Q_B have the Fisher matrix, $F^{(Q)}_{BB'} = \Sigma_{\ell\ell'} F^{(q)}_{\ell\ell'}$, where the sum over ℓ extends across bin B and the sum over ℓ' extends across bin B'. We see that Q_B averages q_ℓ over the filter $f^{(q)}_{B\ell} = \Sigma_{\ell'} F^{(q)}_{\ell\ell'}$. The (q) superscript indicates that this filter is for averaging q_ℓs.

As the constraints on the power spectrum become tighter, it is inevitable that we will move from plotting averages of $\mathcal{C}_\ell$ (band-powers) to plotting q_ℓ in what we call q-space, or deviation space. We show some examples of this later in Section VII where we simulate future data sets. Therefore it is worth exploring this space a little further. One question to answer is: what ℓ value should be used for locating Q_B horizontally on a graph? We advocate choosing this $\ell_{\rm eff}$ so that for a band ranging from ℓ_1 to ℓ_2

$$\sum_{\ell=\ell_1}^{\ell_{\rm eff}} f^{(q)}_{B\ell} = \sum_{\ell=\ell_{\rm eff}}^{\ell_2} f^{(q)}_{B\ell}. \tag{4.4}$$

With this definition, 50% of the weight that constrains q_B comes from $\ell_1 < \ell < \ell_{\rm eff}$ and the other 50% comes from $\ell_{\rm eff} < \ell < \ell_2$.

Although comparison of theories with the data will occur in q-space, we wish to translate our values into the familiar $\mathcal{C}_\ell$-space. To do this we must define a suitable average of $\mathcal{C}_\ell^{\rm shape}$ over bin B, $\mathcal{C}_B^{\rm shape}$, with which to multiply Q_B and a suitable ℓ value at which to plot the error bar, $\ell_{\rm eff}$. The best weighting to use for this is debatable. We emphasize that the ambiguities associated with the translation from Q_B to a power estimate, $\mathcal{C}_B$ only affect plotting—not the comparison of theory with data. Furthermore, we have tried several different weighting schemes and found negligible differences in their values of $\ell_{\rm eff}$ and $\mathcal{C}_B$, so long as they are proportional to $f^{(q)}_{B\ell}$ which encodes the signal-to-noise information in the band.

To motivate a particular averaging we first rewrite Eq. (4.3) in terms of $\mathcal{C}_\ell$ and its Fisher matrix:

$$Q_B = \frac{\sum_{\ell\ell'} \mathcal{C}_\ell F^{(\mathcal{C})}_{\ell\ell'} \mathcal{C}_{\ell'}^{\rm shape}}{\sum_{\ell\ell'} \mathcal{C}_\ell^{\rm shape} F^{(\mathcal{C})}_{\ell\ell'} \mathcal{C}_{\ell'}^{\rm shape}}. \tag{4.5}$$

The relation between Q_B and $\mathcal{C}_\ell$ in the above equation suggests that the following filter be used to calculate $\mathcal{C}_B^{\rm shape}$:

$$f^{(\mathcal{C})}_{B\ell} = \sum_{\ell'} F^{(\mathcal{C})}_{\ell\ell'} \mathcal{C}_{\ell'}^{\rm shape} = f^{(q)}_{B\ell} / \mathcal{C}_\ell^{\rm shape} \tag{4.6}$$

since this is the weighting of each $\mathcal{C}_\ell$ in Eq. (4.5). Therefore to make our power estimates we use

$$\mathcal{C}_B^{\rm shape} = \frac{\sum_\ell f^{(\mathcal{C})}_{B\ell} \mathcal{C}_\ell^{\rm shape}}{\sum_\ell f^{(\mathcal{C})}_{B\ell}} \tag{4.7}$$

with the result that

$$\mathcal{C}_B = Q_B \mathcal{C}_B^{\rm shape} = \frac{\sum_\ell f_{B\ell}^{(\mathcal{C})} \mathcal{C}_\ell}{\sum_\ell f_{B\ell}^{(\mathcal{C})}}. \tag{4.8}$$

The role of the filter function, $f_{B\ell}^{(\mathcal{C})}$ is exactly that of W_ℓ/ℓ in the band-power procedure of [15], where W_ℓ is the trace of the window function matrix defined in Eq. (2.8). We will develop this connection more later. For now, we define $\ell_{\rm eff}$, ℓ^+ and ℓ^-, exactly as was done in [15], so that we can plot data points properly located in ℓ space with horizontal error bars:

$$\ell_{\rm eff} = \frac{\sum_\ell \ell f_{B\ell}^{(\mathcal{C})}}{\sum_\ell f_{B\ell}^{(\mathcal{C})}} \tag{4.9}$$

and ℓ^- and ℓ^+ are where $l f_{B\ell}^{(\mathcal{C})}$ has fallen to $e^{-1/2}$ of its maximum value. We remind the reader that every sum over ℓ in this section is only over the values of ℓ within band B.

B. Initial binning

One may wish to estimate fewer parameters than every multipole moment right from the beginning. In this case one would parameterize the spectrum as

$$\mathcal{C}_\ell = q_B \mathcal{C}_\ell^{\rm shape} \chi_B(\ell) \tag{4.10}$$

where $\chi_B(\ell)$ is one, when ℓ is within the range of band B, and zero otherwise.

To convert q_B to a power estimate, $\mathcal{C}_B$, we need an average of the shaped spectrum over band B. A useful conversion factor is given by Eq. (4.7). Of course, in order to calculate $\mathcal{C}_B^{\rm shape}$ by Eq. (4.7) one needs to know the Fisher matrix at every ℓ—which is a calculation we are trying to avoid by using coarse binning. Once again though, as long as the binning is not too coarse, the details of the averaging are unimportant. If the binning is fine enough, then a simple average (uniform in ℓ) will suffice—that is, take

$$\mathcal{C}_B^{\rm shape} = \frac{\Sigma_\ell \mathcal{C}_\ell^{\rm shape} \chi_B(\ell)}{\Sigma_\ell \chi_B(\ell)}; \tag{4.11}$$

here, the denominator is simply the width of the bin. This is what we have done in our applications (although see Section VI for how this can be improved by use of analytic knowledge of the Fisher matrix).

As is usually the case with binning, we want to make the bins as fine as necessary to capture all the information, but no finer since that means extra work. A lower limit to the bin sizes comes from the fact that fluctuation power from $\mathcal{C}_\ell$ will be indistinguishable from that from $\mathcal{C}_{\ell'}$ if $|\ell - \ell'| \lesssim 2\pi/\theta$, where θ is the linear extent of the observed region, as already mentioned. We may wish to make our initial bins even coarser. Some considerations to keep in mind are that if one is trying to reduce sensitivity to uncertainty in the power-law index, then logarithmic spacing produces equal shape sensitivity in each bin. If the chief shape uncertainty comes from features with a characteristic wavelength, *e.g.*, Doppler peaks, then a linear spacing produces equal shape sensitivity in each bin.

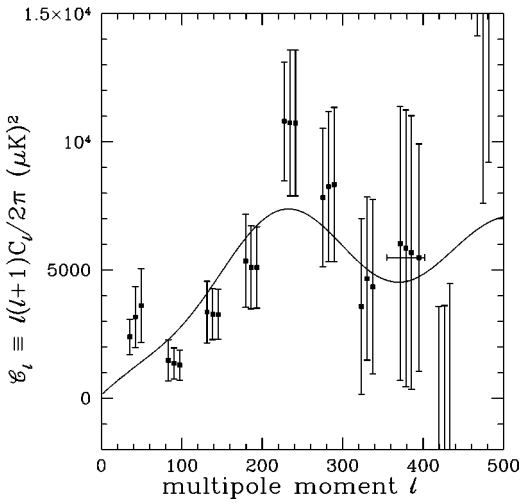

FIG. 8. Quadratic estimates of the power in 10 bins, derived from the SK data. The curve is the zeroth iteration, tilted CDM with $n = 1.45$ and $\sigma_8 = 2.16$. The squares are from left to right, the results of the first to third iterations. The data point with the horizontal error bar is a rebinning of the top three bins.

V. APPLICATION TO SASKATOON

We now apply our methods to the Saskatoon (SK) dataset [11]. The SK data are reported as complicated chopping patterns (*i.e.*, beam patterns, H, above) in a circle of radius about 8° around the North Celestial Pole. The data were taken over 1993–1995 (although we only use the 1994–1995 data) at an angular resolution of 1.0–0.5° full width at half maximum (FWHM) at approximately 30 GHz and 40 GHz. More details can be found in [11]. The combination of the beam size, chopping pattern, and sky coverage mean that SK is sensitive to the power spectrum over the range $\ell = 50$–350. The Saskatoon dataset is calibrated by observations of supernova remnant, Cassiopeia-A. Leitch and collaborators [28] have recently measured the flux and find that the remnant is 5% brighter than the previous best determination. We have adjusted the Saskatoon data accordingly.

In Fig. 8 we show the results of our iterated quadratic estimator on the SK data, in ten evenly spaced bins from $\ell = 19$ to $\ell = 499$. Again, the convergence proceeds quite rapidly, although not quite as rapidly as for COBE DMR. Evaluation of the Fisher matrix shows that there are approximately 20% anti-correlations between neighboring bins. We note in passing that the falling power spectrum seen for $\ell \lesssim 100$ has been noticed by the experimenters themselves [29].

What we directly estimate is the adjustment factor q_B of Eq. (4.10). As mentioned above, in order to convert this to a power spectrum amplitude, we need some measure of the average power in the bin. Here we have used an average uniform in $\mathcal{C}_\ell$ across the bin [Eq. (4.11)]. For the first bin, the averaging should probably be weighted more to the higher multipole moments than to the lower ones in the bin because the sensitivity to the spectrum is increasing rapidly

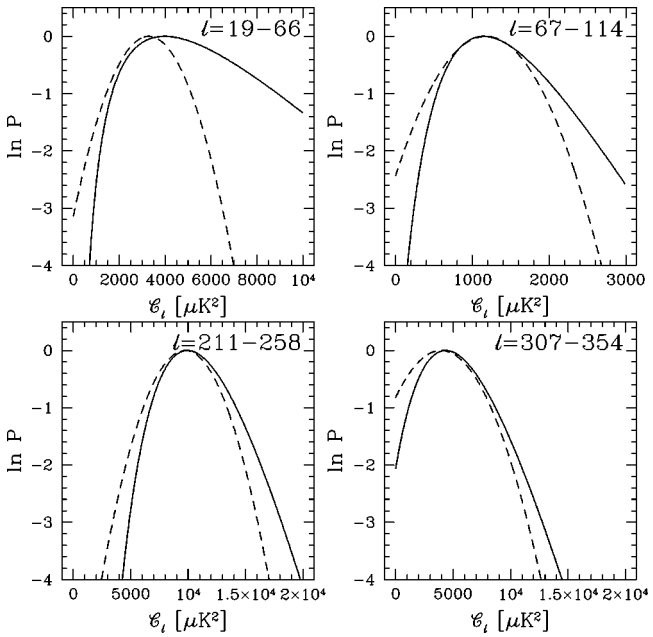

FIG. 9. Probability distributions for the power in bands, $\mathcal{C}_B$, as labeled, for a prior uniform in $\mathcal{C}_B$. The solid curve is the true likelihood from the direct evaluation; the dotted curve is the Gaussian approximation from the third iteration of the quadratic procedure.

with increasing ℓ. We will see this rapid rise in sensitivity to the power spectrum in the next section where we plot the Fisher matrix for a finer binning.

There is very little information in the three highest ℓ bins. Thus, for the final iteration we binned them together and plotted the result as the point with the horizontal error bar. Because of the coarseness of the bins, the filter function for the rebinning is coarse and therefore $\ell_{\rm eff}$, ℓ^+ and ℓ^- are not determined very well. To get the filter function more finely, we need to do a finer initial binning, which will be done in the next section.

To investigate the probability distributions beyond the mean and the variance, we used our direct likelihood evaluation procedure, starting from the final quadratic iteration. The results are shown in Fig. 9. The uncertainties in the first bin are strongly sample-variance dominated. In the sample-variance limit the fractional variance, $(\delta\mathcal{C}_\ell)^2/\mathcal{C}_\ell^2$, is inversely proportional to the number of independent modes contributing to the estimate. Since the first bin is not well-determined we can therefore surmise that only a few modes contribute to it. With so few modes we cannot expect the distribution to be Gaussian and thus the strong non-Gaussianity for the first band, shown in Fig. 9, is not surprising.

VI. METHODS: RADICAL COMPRESSION

As mentioned above, for Gaussian theories, $P(\Delta|\mathcal{C}_\ell)$ contains all the information that is in the map. If the probability distribution were Gaussian in $\mathcal{C}_\ell$, then all the information in the probability distribution could be compressed into a mean and a covariance matrix:

$$P(\Delta|\mathcal{C}_\ell)\rightarrow\hat{\mathcal{C}}_\ell,\langle\delta\mathcal{C}_\ell\delta\mathcal{C}_{\ell'}\rangle. \tag{6.1}$$

By the definition of a Gaussian probability distribution, this compression involves no loss of information. The ''lossless'' nature of this compression was pointed out by Tegmark [7], although here we emphasize that it is only true in the Gaussian limit. We refer to compression to the power spectrum as ''radical compression'' because the data reduction is impressive: the information in a map with N pixels and an $N\times N$ noise covariance matrix is now held in less than $\sqrt{N}$ power estimates and their $\sqrt{N}\times\sqrt{N}$ covariance matrix.

With compression to $\sqrt{N}$ numbers and a covariance matrix, analysis of constraints on cosmological parameters becomes quite rapid. One simply forms the χ^2:

$$\chi^2(\{a\})=\sum_{\ell\ell'}(\mathcal{C}_\ell(\{a\})-\hat{\mathcal{C}}_\ell)M^{-1}_{\ell\ell'}(\mathcal{C}_{\ell'}(\{a\})-\hat{\mathcal{C}}_{\ell'}) \tag{6.2}$$

and simply evaluates it to find the minimum and also the one sigma and possibly two sigma confidence regions of the parameter space. Here, $\mathcal{C}_\ell(\{a\})$ is the calculated spectrum for the paramters a_p and $M_{\ell\ell'}\equiv\langle\delta\mathcal{C}_\ell\delta\mathcal{C}_{\ell'}\rangle$ is some appropriately determined correlation matrix, *e.g.*, the inverse of the Fisher matrix or the exact curvature matrix for the quadratic method, or a likelihood ratio or Bayesian determination for the direct evaluation of the likelihood.

Unfortunately, the probability distribution is non-Gaussian, as we have seen. One might think that this only causes minor inaccuracies to the method of Eq. (6.2). In fact, the problems are of a systematic nature and can be quite important. To see this we need only examine the case of COBE DMR. Say we wanted to use our power spectrum estimates to measure the best fit amplitude of standard CDM, expressed as a prediction for σ_8, by using Eq. (6.2). Using our estimates of $\mathcal{C}_\ell$ from the final iteration of either the direct or quadratic estimation procedures together with the Fisher matrix from the final iteration, we find $\sigma_8=1.1$ instead of the correct value of $\sigma_8=1.2$. This example does not mean that non-Gaussianity has made radical compression useless, but rather that we must proceed with some care.

The decrease in power is a systematic effect due to the skewness of the probability distributions which allow more positive and less negative fluctuations relative to a Gaussian distribution with the same variance. Another way of thinking about it is that those amplitudes that fluctuate downwards have their variance reduced and thus their weight increased, while those that fluctuate upward have their variance increased and therefore their weight decreased. Contrast this to a Gaussian probability distribution for which the curvature is independent of location. Thus one can see that the non-Gaussianity of the probability distribution can be very important and some care must be used in attempting this radical compression.

One solution to the problem may be to find a function of $\mathcal{C}_\ell$ whose distribution is more Gaussian than that of $\mathcal{C}_\ell$ itself. Motivation for one particular form comes from considering the sources of the variance. There is a sample-variance contribution which is proportional to the power and a noise contribution which is independent of the power, thus $\delta\mathcal{C}_\ell\propto\mathcal{C}_\ell+x_\ell$ for some appropriate x_ℓ related to the experimental noise. According to this proportionality, the probability distribution for $\ln(\mathcal{C}_\ell+x_\ell)$ might be well approximated by a

Gaussian since its variance is independent of $\mathcal{C}_\ell$. This procedure is under investigation [4].

It is the iterated Fisher matrix that overweights (underweights) the points that fluctuated downward (upward); to prevent these fluctuations from affecting the Fisher matrix, one can iterate on the parameters of a smooth function, instead of the amplitudes in fine bins, and then use the resulting Fisher matrix for the covariance matrix associated with the power estimates in bins. This is the method of solution we have adopted here.

We emphasize that the problems we are discussing are not peculiar to the use of the quadratic estimator, but are associated with the attempt to compress the probability distribution of $\mathcal{C}_\ell$ into a mean and covariance matrix. Because of non-Gaussianity, this procedure is necessarily approximate. The above being said, we will now assume Gaussianity, but always use the Fisher matrix derived from a smooth theory curve, and not one derived from a bin by bin iteration.

A more benign problem than non-Gaussianity is the existence of correlated uncertainties. Although not a problem for the χ^2 of Eq. (6.2), the correlations do complicate direct visual interpretation. We may remove these correlations by a linear transformation on the parameter space, $q \to \widetilde{q} = Zq$, where Z diagonalizes the parameter covariance matrix, $ZF^{-1}Z^T = diag$ (or, equivalently, Z^{-1} diagonalizes the Fisher matrix, $F^{(q)}$).

While having the advantage of uncorrelated uncertainties, the interpretation of these new parameters themselves has been complicated by the transformation. Fortunately, there are transformations with some very useful properties. Many transformations can lead to independent modes. Hamilton [22] made a lengthy study of the different possible diagonalizing transformations and found one that has a small ℓ-space width and is positive-definite. His transformation translates to $Z = L^T$, where L is the Cholesky factorization of F; $F = LL^T$. Another useful transformation is given by setting $Z = F^{1/2}$, the Hermitian square root of F [23]. Parameter eigenmodes [3], involving rotation only to the orthogonal combinations of bandpowers, rather than scale transformations as well, are of great interest and emphasize another point: when linear combinations of modes are being taken, we have freedom in exactly what the scaling will be. It is obvious though that if we are representing a bandpower at a representative ℓ, we want to ensure that the normalization makes sense since the goal is direct visual comparison with theoretical $\mathcal{C}_\ell$ curves.

In the Gaussian approximation, these linear combinations are independent. Thus we can now estimate each $\widetilde{q}_j$ independently of the $\widetilde{q}_i$ for $i \neq j$. The ℓ_{max}-dimensional space has been reduced to ℓ_{max} one-dimensional spaces. In fact, for each $\widetilde{q}_j$, there is no need to keep the Gaussian approximation; one can calculate its complete distribution function. If the Fisher matrix is a good approximation to the curvature matrix, then, at least near the peak, the total likelihood function can be approximately decomposed into a product of these one-dimensional likelihood functions: $\mathcal{L}(\{\widetilde{q}_i\}) \approx \Pi_i \mathcal{L}(\widetilde{q}_i)$. Since $\widetilde{q}_\lambda = q_\ell Z_{\ell\lambda} = \mathcal{C}_\ell / \mathcal{C}_\ell^{\rm shape} Z_{\ell\lambda}$, the filter function is $f_{\lambda\ell}^{(\mathcal{C})} = Z_{\ell\lambda} / \mathcal{C}_\ell^{\rm shape}$. Thus

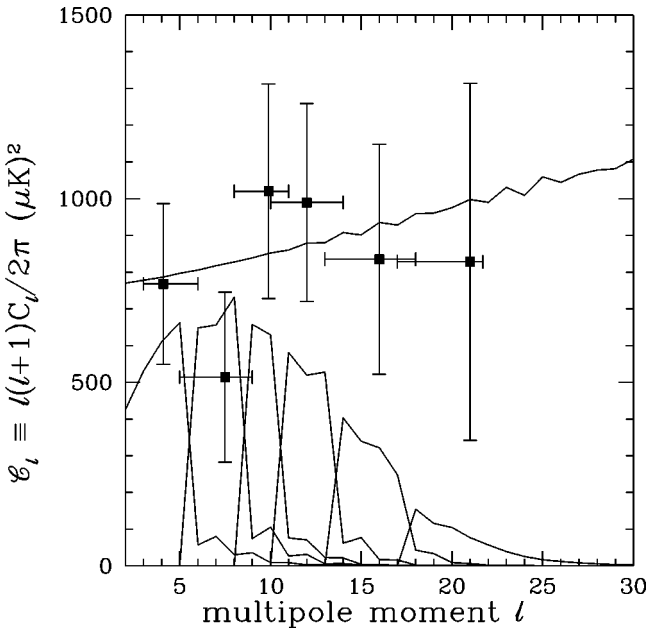

FIG. 10. DMR with ortho-rebinning.

$$\mathcal{C}_\lambda = \frac{\widetilde{q}_\lambda}{\sum_\ell f_{\lambda\ell}^{(\mathcal{C})}} = \frac{\sum_\ell \mathcal{C}_\ell f_{\lambda\ell}^{(\mathcal{C})}}{\sum_\ell f_{\lambda\ell}^{(\mathcal{C})}}. \tag{6.3}$$

If we wish to rebin these uncorrelated estimates, we can do so in a minimum variance manner by performing the following sums:

$$\mathcal{C}_\beta = \frac{\sum_{\lambda \in \beta} \widetilde{q}_\lambda N_\lambda}{\sum_\ell f_{\beta\ell}^{(\mathcal{C})}} \tag{6.4}$$

where

$$f_{\beta\ell}^{(\mathcal{C})} = \sum_{\lambda \in \beta} f_{\lambda\ell}^{(\mathcal{C})} N_\lambda \tag{6.5}$$

and $N_\lambda \equiv \Sigma_\ell Z_{\ell\lambda}$. These equations are derived in Appendix B.

For COBE DMR we used Cholesky decomposition to get filter functions, $f_{\lambda\ell}^{(\mathcal{C})} = L_{\ell\lambda} / \mathcal{C}_\ell^{\rm shape}$, and then binned together combinations 1-3,4-5,6-7,8-9,10-12,13-16 and 17-27. Each of the combinations' filter functions is shown in Fig. 10, together with the power estimates. To avoid the systematic underestimate of power discussed above, we used the $\mathcal{C}_\ell$s from our final iteration, but the Fisher matrix from the zeroth iteration. This does not imply that the errors are completely unaffected by the data. We are using standard CDM as our zeroth iteration precisely because it is a good fit to the data.

In order to make accurate filter functions for SK we divided it up into 26 bins. Starting from the results of our third iteration on the 10 bands of the previous section, we estimated the power in these 26 bands with a single iteration. The fractional uncertainty in most of these bands was greater

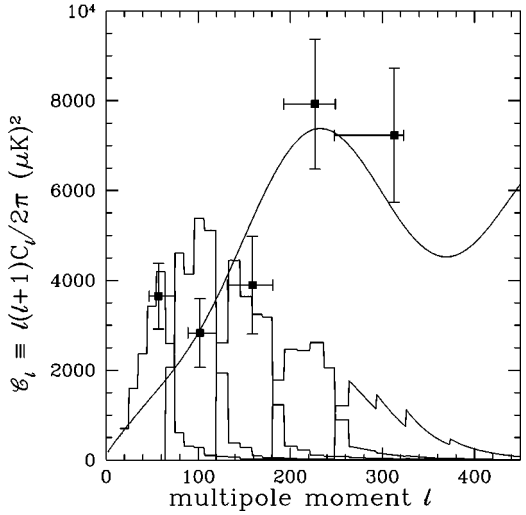

FIG. 11. SK with ortho-rebinning.

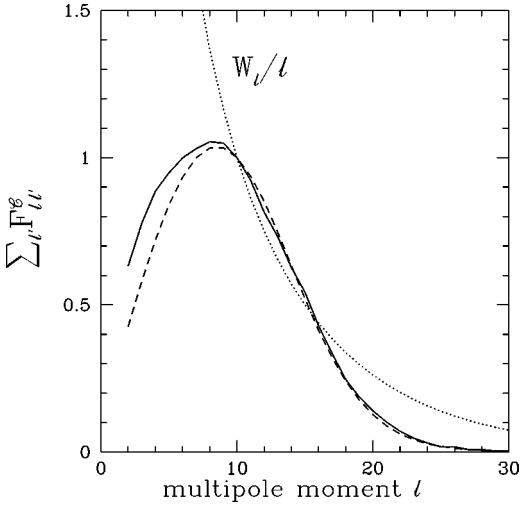

FIG. 12. The Fisher matrix sum, $\Sigma_{\ell'} F^{(\mathcal{C})}_{\ell\ell'}$, for the zeroth iteration of DMR for exact (solid) and analytic (dashed). For comparison, W_ℓ/ℓ (dotted) is also shown.

than unity. In order to make the rebinned statistically orthogonal linear combinations plotted in Fig. 11 we used the $n=1.45$, $\sigma_8=2.16$ tilted standard CDM Fisher matrix. These are the parameter values for tilted CDM that maximize the likelihood function.

At high ℓ, some of our 26 bands still have significant width; their ''sub-band structure'' may be important. To estimate the structure of the filter functions *within* each band, we employ an analytic approximation to the Fisher matrix. For a map of the sky with uniform weight per solid angle, w, covering a fraction of the sky, $f_{\rm sky}$, we know the Fisher matrix is such that [1–3]:

$$\sum_{\ell'} F^{(\mathcal{C})}_{\ell\ell'} \simeq \frac{(2\ell+1)f_{\rm sky}}{2}\left(\mathcal{C}_\ell + \frac{\ell(\ell+1)}{2\pi w \mathcal{B}^2(\ell)}\right)^{-2}, \quad (6.6)$$

where, for a Gaussian beam, $\mathcal{B}(\ell)=e^{-\ell^2\sigma_b^2/2}$.

An approximation appropriate for difference experiments rather than maps is to replace $w\mathcal{B}^2(\ell)$ with the noise-weighted window function $w\overline{W}^{(N)}_\ell \equiv {\rm Tr}(C_N^{-1}\mathbf{W}_\ell)/N$, where $\mathbf{W}_\ell$ is the window function matrix of Eq. (2.8). In this uniform case, we also have

$$f^{(q)}_{B\ell} \simeq \frac{(2\ell+1)f_{\rm sky}}{2}\left(\frac{\varepsilon_{T\ell}}{(1+\varepsilon_{T\ell})}\right)^2,$$

$$\varepsilon_{T\ell} \equiv w\overline{W}^{(N)}_\ell \mathcal{C}_\ell \frac{2\pi}{\ell(\ell+1)}. \quad (6.7)$$

The quantity $\varepsilon_{T\ell}$ is a measure of the mean square of the signal-to-noise ratio in modes ℓ. The $\varepsilon_{T\ell}/(1+\varepsilon_{T\ell})$ factor which appears in the square is the Wiener filter (*i.e.*, the optimal signal-to-noise filter). In the $\varepsilon_{T\ell}\gg 1$ limit of signal-dominance, $f^{(q)}_{B\ell}\to(\ell+1/2)f_{\rm sky}$, half the number of ℓ modes available. This is of course a general result for the signal-dominated regime, requiring no assumption of homogeneous noise. It is often a reasonable approximation to use the usual filter function $W_\ell \equiv {\rm Tr}(\mathbf{W}_\ell)/N$ in place of the noise-weighted one. Eq. (6.7) is applied to realizations of power spectra for future balloon and satellite experiments in Section VII.

The weight map for COBE DMR varies gently with spatial scale outside of the galactic cut, so we expect the analytic approximation Eq. (6.6) to be reasonably good for it and we see in Fig. 12 that this is so. The two curves with a peak at $\ell=10$ are sums over the exact and analytic Fisher matrices for standard CDM. For the analytic form we took $f_{\rm sky}=0.65$, $w^{-1}=9.5\times10^{-13}$ (equivalent to an rms noise of 22 μK on 7° pixels) and the appropriate beam shape.

For the SK data, the comparison of the 26 band exact Fisher matrix and the analytic Fisher matrix approximation shows some interesting differences (Fig. 13). The analytic curve is for $f_{\rm sky}=0.005$, $w^{-1}=3.3\times10^{-14}$ and $\theta_{\rm fwhm}=0.5°$. The deficit at smaller ℓ is presumably due to the differencing schemes that were necessary to filter out atmospheric contamination. These are partly encoded in the noise-weighted $\overline{W}^{(N)}_\ell$, but for the plot only the beam, $\mathcal{B}^2(\ell)$, was used, as in Eq. (6.6). This deficit bears on the question of what quality of map it is possible to create from the SK dataset; the loss of low ℓ information implies that there will be long-distance noise correlations in any map made from the data [31].

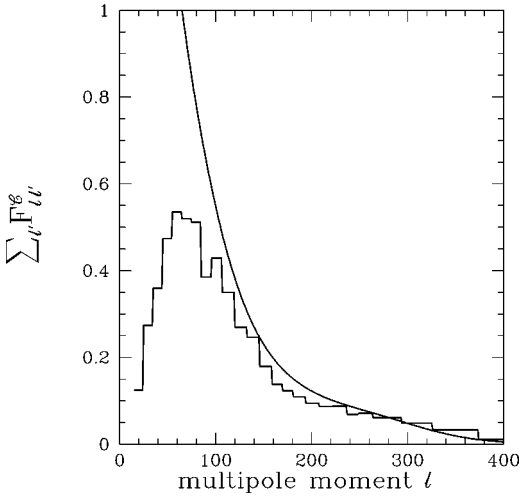

FIG. 13. The Fisher matrix sum, $\Sigma_{\ell'} F^{q}_{\ell\ell'}$, for the zeroth iteration on 26 band SK for exact and analytic.

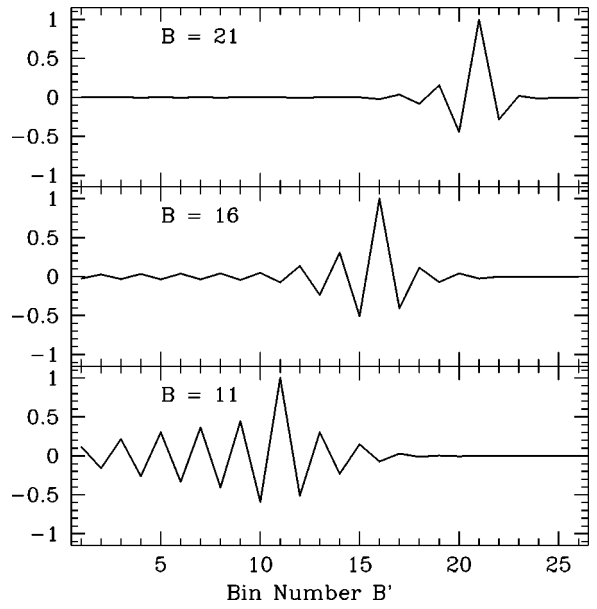

FIG. 14. Slices of the SK 26 band covariance matrix at bands 11, 16 and 21, normalized to unity along the diagonal.

In Fig. 14 we show some rows of the normalized parameter covariance matrix $M_{BB'}/\sqrt{M_{BB}M_{B'B'}}$, where $M_{BB'}=F^{-1}_{BB'}$. The correlations for bin 11 ($\ell=120$–132) extend well beyond the $\delta\ell\simeq\pi/\theta$ expected for a map—again, this is presumably due to the differencing schemes.

Returning to Fig. 13, we see that the agreement at least at higher ℓ, is good. We consider it to be good enough to encourage the use of the analytic form for doing some subband shaping of the filter functions. To be more precise about the procedure, within each band, B, we give $f^{(\mathcal{C})}_{\beta\ell}$ the shape $\Sigma_{\ell'}f^{(\mathcal{C})}_{\ell\ell'}\mathcal{C}_{\ell}$ with the amplitude chosen so that $f^{(\mathcal{C})}_{\beta B}=\Sigma_{\ell}f^{(\mathcal{C})}_{\beta\ell}$. We have applied this shaping to the five highest ℓ bins in Fig. 11.

One might wonder why the analytic curve in Fig. 13 has no peak, corresponding to where sample variance and noise are equal contributors to the uncertainty in $\mathcal{C}_{\ell}$. The absence of the peak is due to the rise in $\mathcal{C}_{\ell}$ from $\ell=20$ to $\ell=200$. If we plotted $\mathcal{C}^2_{\ell}\Sigma_{\ell'}F^{(\mathcal{C})}_{\ell\ell'}$, which is related to the *fractional* uncertainty in $\mathcal{C}_{\ell}$, then there would be a peak near $\ell=80$.

While the independence of the power estimates (in the Gaussian approximation) simplifies Eq. (6.2) some, the existence of the filter functions complicates it:

$$\chi^2(\{a\})\equiv\sum_B\frac{1}{(\delta\mathcal{C}_B)^2}[\mathcal{C}_B(\{a\})-\hat{\mathcal{C}}_B]^2, \qquad (6.8)$$

where $\mathcal{C}_B(\{a\})$ is calculated using the filters in Eq. (4.7). We have cast this equation in an intuitive form involving the deviation of a measured bandpower $\mathcal{C}_B$ from the predicted spectrum. This is exactly the χ^2 appropriate to q-space, which emphasizes relative deviations of both the data and the theoretical predictions from the fiducial spectrum used to calculate the quadratic estimator; *i.e.*, the details of how one goes from the estimates of q_B to the appropriate bandpower drop out of the χ^2.

One might argue that the complication of the covariance matrix has been traded for the complication of the filter functions and there has been no net improvement. However, we think that, when binning has been done, the use of the orthogonal linear combinations improves, or at least simplifies, the process of radical compression. Once binning has occurred, one wants to know what the filter looks like across the bin. Thus binning implies the use of filters and once filters are being used, the orthogonal linear combination approach of providing uncorrelated data and filters is simpler than providing correlated data with filters *and* a covariance matrix.

Experiments typically report broad-band power spectrum estimates, together with the trace of their window function, W_{ℓ}, which can be used to make a filter function, $f_{\ell}=W_{\ell}/\ell$. These power spectrum estimates have indeed been used to constrain cosmological parameters, *e.g.* [12]. Using $f_{\ell}=W_{\ell}/\ell$ as the filter function is in general not the optimal procedure. Only if $C_{Tii'}$ is a multiple of the identity matrix is W_{ℓ}/ℓ the minimum-variance filter. In general, the Fisher matrix-derived filters should be used. And they can be quite different; in Fig. 12 one can see the tremendous difference between W_{ℓ}/ℓ and the minimum variance filter, f_{ℓ}. In the noise-dominated regime (high ℓ for DMR), $W_{\ell}/\ell\propto\ell^{-1}B^2(\ell)$ whereas $f_{\ell}\propto\ell^{-3}B^4(\ell)$.

In our power spectrum plots we have not included calibration uncertainty which is $\sim 6\%$ for SK and negligible for COBE DMR. The calibration uncertainty is completely correlated across the bands. It can be taken into account as a nuisance parameter to be added to the χ^2 expression above [12]. Other methods for taking it into account are discussed in [4].

VII. FORECASTING POWER SPECTRA FOR FUTURE EXPERIMENTS

In this section, we exercise our methods on an instructive simple case, homogeneous noise over regular patches covering a fraction $f_{\rm sky}$ of the sky. We apply the relations to simulating realizations of power spectra and their error bars for two planned balloon experiments, MAXIMA and TOPHAT, and two satellite experiments, Microwave Anisotropy Probe (MAP) and PLANCK. The results are shown in the familiar $\mathcal{C}_{\ell}$ space in Fig. 15 and in $\Delta\mathcal{C}_{\ell}/\mathcal{C}_{\ell}$ space in Fig. 16. In this q-space, which we believe will become more and more utilized as the CMB data starts to converge on a specific shape, we compare the (converged) quadratic power estimator values and their error bars with the fractional deviation, $\Delta\mathcal{C}_{\ell}/\mathcal{C}_{\ell}$, of a $\mathcal{C}_{\ell}$ whose parameters we are testing from a fiducial shape. Here the shape that entered into the power spectrum analysis was a standard COBE-normalized cold dark matter model $\mathcal{C}_{\ell}$, and the model used to construct the power spectrum realization was also this standard CDM one.

For $f_{\rm sky}=1$, power spectrum analysis simplifies considerably if the weight matrix C_N^{-1} is diagonal in the spherical harmonics basis, since then the C_T and $C_{T,p}$ matrices are. Both the Fisher and curvature matrices are also diagonal as long as the bands B do not overlap in ℓ-space. For $f_{\rm sky}<1$, another simple limiting case involves rectangular regions of size $N_x\varpi_{pix}\times N_y\varpi_{pix}$, consisting of square pixels of size $\varpi_{pix}\times\varpi_{pix}$. The S/N eigenmodes are then discrete Fourier components, labelled by a wave vector $\mathbf{Q}$, which, to a high degree of accuracy, diagonalize C_T and $C_{T,p}$, and, by as-

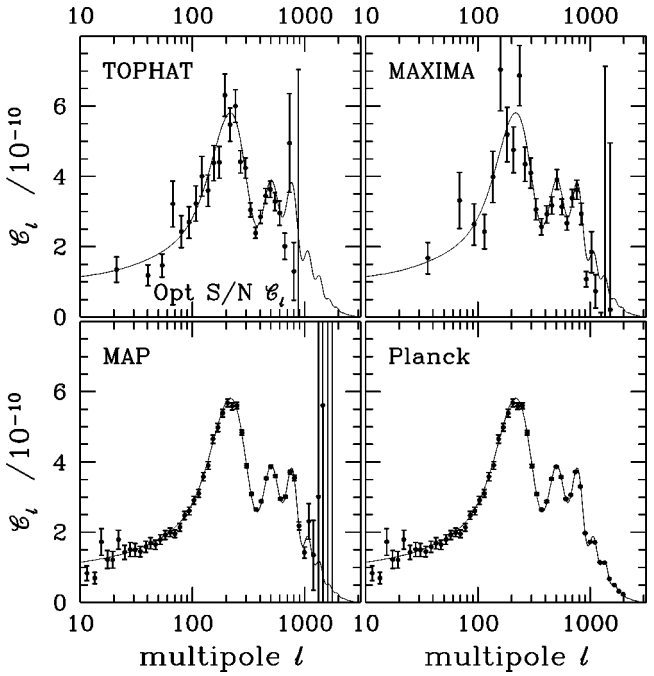

FIG. 15. Comparison of forecasts for the two balloon experiments, TOPHAT and MAXIMA, with the satellite experiments MAP and PLANCK. Bands are required to have a signal-to-noise of at least 25 and a minimum spacing in ℓ defined by the logarithmic spacing $\Delta\ln\ell=0.1$. With this signal-to-noise binning, the growth in the number of bands shows the increasing precision and sky coverage of the experiments. The error bars are those appropriate to the quadratic estimator after convergence.

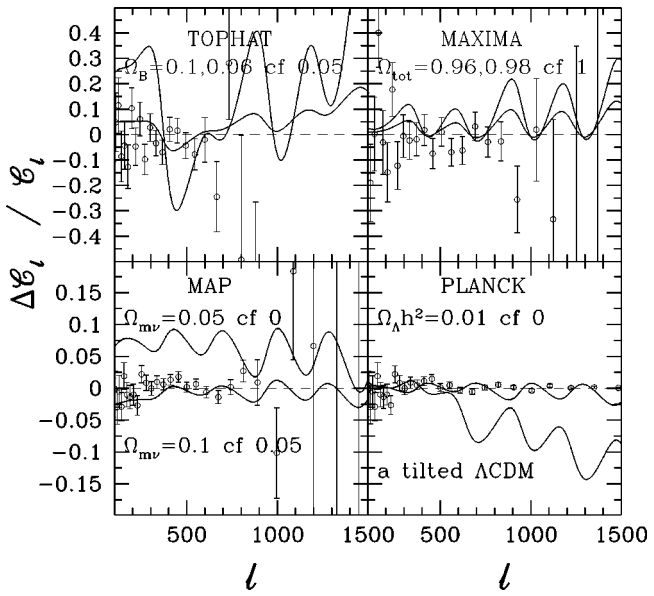

FIG. 16. The forecasted data with error bars are shown in ($q=\Delta\mathcal{C}_\ell/\mathcal{C}_\ell$)-space, in which the relevant comparison with the data is the fractional difference between the $\mathcal{C}_\ell$ we are testing and $\mathcal{C}_\ell^{shape}$. A few differences are shown for each case by solid lines. They are deviations in single parameters, as marked, from the shape theory ($q=0$), in this case a standard COBE-normalized CDM model with $\Omega_B=0.05$. The theoretical curves can have their amplitudes adjusted up or down to best fit the simulated data.

sumption, C_N^{-1}. The number of modes of a given $|\mathbf{Q}|$ available in a $d|\mathbf{Q}|=1$ band is $[N_xN_y\varpi_{pix}^2/(2\pi)]|\mathbf{Q}|$; *i.e.*, $f_{\rm sky}2|\mathbf{Q}|$. Using $|\mathbf{Q}|\approx\ell+\frac{1}{2}$, which follows from relating an expansion in these modes to an expansion in spherical harmonics at high ℓ [30], the number of modes is $(2\ell+1)f_{\rm sky}$, as in the all-sky case.

The Fisher matrix and the quadratic q-estimator are given by

$$\delta Q_B=v_B/(2F)_{BB},\quad F_{BB}=\sum_{\ell\in B}f_{B\ell}^{(q)},\tag{7.1}$$

$$v_B=\sum_{\ell\in B}2f_{B\ell}^{(q)}\frac{[(1+\varepsilon_{T\ell}^{\rm true})\rho_\ell^2-(1+\varepsilon_{T\ell}^{(*)})]}{\varepsilon_{T\ell}^{(*)}},$$

$$2f_{B\ell}^{(q)}\equiv g_\ell[\varepsilon_{T\ell}^{(*)}/(1+\varepsilon_{T\ell}^{(*)})]^2,\quad g_\ell\equiv(2\ell+1)f_{\rm sky}.$$

The signal-to-noise factor $\varepsilon_{T\ell}$ is related to the average weight w, the noise-weighted filter function $\overline{W}_\ell$, and $\mathcal{C}_\ell$ by Eq. (6.7); and the expression for $f_{B\ell}^{(q)}$ is a repeat of Eq. (6.7). It is also straightforward to modify $\varepsilon_{T\ell}$ to take into account the noise in multifrequency experiments, including the expected beam size variation with frequency channel [3].

The combination $(1+\varepsilon_{T\ell}^{\rm true})\rho_\ell^2$ is the average power in the modes with given ℓ, where $\varepsilon_{T\ell}^{\rm true}$ is the true value of the power spectrum, and

$$\rho_\ell^2=g_\ell^{-1}\sum_{\mu\in\{\ell-\rm modes\}}{\rm GRD}_{\ell\mu}^2,$$

where ${\rm GRD}_{\ell\mu}$ is a Gaussian random deviate for the mode of given ℓ labelled by a degeneracy variable μ (the azimuthal quantum number, m, in the spherical harmonic case, a discrete angle index in the rectangular patch case); individual realizations of this variable are due to sample and/or cosmic variance. Therefore, $g_\ell\rho_\ell^2$ is distributed like χ^2 with g_ℓ degrees of freedom, *i.e.*, with a cumulative probability given by an incomplete Gamma function with arguments $g_\ell/2$ and $\rho_\ell^2/2$. Numerical realizations can be done very quickly.

The factor $\varepsilon_{T\ell}^{(*)}$ denotes an approximate value for the signal-to-noise power spectrum. As we have discussed, within the band we adopt an assumed shape, but allow the amplitude Q_B to vary. In the iterative scheme, $\varepsilon_{T\ell}^{(*)}=\varepsilon_{T\ell}^{(n)}$ would be the value on iteration n, and $\varepsilon_{T\ell}^{(n+1)}=(1+\delta Q_B)\varepsilon_{T\ell}^{(n)}$ would be the value to be inserted for the next iteration.

Note that Q_B is the weighted average of the quadratics in sub-bands of width unity, Q_ℓ, with weight $f_{B\ell}^{(q)}$. Therefore, the classic optimal signal-to-noise filter, the Wiener filter, $\varepsilon_{T\ell}/(1+\varepsilon_{T\ell})$ in this case, enters in a fundamental way into the power spectrum estimation procedure.

In the signal-dominated region, $\varepsilon_{T\ell}\gg1$, the weighting is just by number of modes, $2f_{B\ell}^{(q)}\to g_\ell$. Thus F does not change, and δQ_B converges after one iteration. The $\mathcal{C}_\ell$ error bars change because the $\langle\mathcal{C}_\ell\rangle_B$ is multiplied by the converged $(1+\delta Q_B)$. In the fine-grained case, where B encompasses just one ℓ, the $f_{B\ell}^{(q)}$ weights in the v_B numerator and

the Fisher denominator cancel, leaving $1+\varepsilon_{T\ell}^{(n)} = (1+\varepsilon_{T\ell}^{\rm true})\rho_\ell^2$ for $n\geq 1$ even in the noise-domimated regime.

We adopt improved specifications especially in beam size for MAP [32] and PLANCK [33] over the original proposal values; these are likely to evolve for PLANCK. Of the 5 High Electron Mobility Transistor (HEMT) channels for MAP, we assume the three highest frequency channels, at 40, 60 and 90 GHz, will be dominated by the primary cosmological signal (with 30 and 22 GHz channels partly contaminated by bremsstrahlung and synchrotron emission). MAP also assumes 2 years of observing. For PLANCK, 14 months of observing and current (proposal-modified) values are used. The HEMT-based Low Frequency Instrument (LFI) specifications are significantly improved; the 100, 65, 44 GHz channels, but not the 30 GHz channel, were used. For the bolometer-based High Frequency Instrument (HFI), 100, 150, 220 and 350 GHz were used. Dust-contamination will certainly affect the 550 and 850 GHz channels. For both, it was assumed that 65% of the sky would be useful. MAP has $w^{-1}=0.8\times 10^{-15}$ and PLANCK has $w^{-1}=3.3\times 10^{-18}$.

The balloon forecasts used conservative numbers for the bolometer-based TOPHAT [34] and MAXIMA [35] experiments that take account of excess noise associated with foreground removal. It was assumed that 65% of the region covered by TOPHAT would be useable for CMB analysis ($f_{\rm sky}=0.028$). The beam is $20'$ and $w^{-1}=1.5\times 10^{-15}$ was chosen. (These noise values are for roughly a 10 day mission.) MAXIMA has a $12'$ beam, and $f_{\rm sky}=0.01$, $w^{-1}=0.9\times 10^{-15}$ were chosen.

Other long duration balloon (LDB) bolometer experiments such as BOOMERANG [36] should be able to do as well. HEMT-based LDB experiments, such as BEAST [37] using 40 GHz HEMTs, might also achieve similar accuracy. A sharp lower ℓ-cut was included to treat the limited sky coverage for TOPHAT ($\ell_{cut}=12$) and MAXIMA ($\ell_{cut}=20$); we allowed one mode per ℓ above this until $(2\ell+1)f_{\rm sky}$ exceeded unity, at which point the number of modes was given by the integer part of $(2\ell+1)f_{\rm sky}$. An uncertain part of this approach is the treatment of modes of order the size of the patch.

In Fig. 15, we have tested various prescriptions for placing the power and the ℓ value. In Section IV A, we recommended using $f_{B\ell}^{(\mathcal{C})}=2f_{B\ell}^{(q)}/\mathcal{C}_\ell$, but other schemes can also be defended; *e.g.*, weighting by the power in the modes, so the numerator averages $[\ell(\ell+1)]^{-1}\mathcal{C}_\ell\ wrt\ f_{B\ell}^{(q)}$ and the denominator averages $[\ell(\ell+1)]^{-1}$. For a steeply falling spectrum, the former places the error bar at high ℓ, with power weighting it is placed at slightly lower ℓ. In all cases, $f_{B\ell}^{(q)}$ is essential to include, but, apart from this, the main lesson we have learned is that otherwise the prescription does not matter very much.

The decision on the number and placement of bands has also been explored. We prefer using a combination of conditions to determine the spacing: when the S/N estimate $v_B/(2\sqrt{F_{BB}})$ exceeds some threshold, or if $\Delta\ln\ell$ across the band reaches some prescribed value, then a new band is made. If we only used logarithmic spacing, then there would be too many bands at lower ℓ with poorly determined bandpowers for TOPHAT and MAXIMA. For the figures, we chose a S/N minimum of 25, translating to a 20% fractional error on $\mathcal{C}_\ell^{1/2}$; we also chose $\Delta\ln\ell=0.1$. Clearly, because of the all-sky nature of MAP and PLANCK, the bands are mostly determined by the logarithmic criterion. This is only true at the higher ℓ (but before the beam kicks in) for the balloon experiments.

One of the nice features of the homogeneous sky simplicity is that we can easily test what different prescriptions and weightings will do. For example, we have explored other ways of finding the maximum and estimating the errors. The nonlinear maximum likelihood estimator uses the curvature matrix:

$$\delta Q_B(\max\mathcal{L})=v_B/(2\mathcal{F})_{BB}, \tag{7.2}$$

$$\mathcal{F}_{BB}=F_{BB}+\sum_\ell 2f_{B\ell}^{(q)}\ \frac{(1+\varepsilon_{T\ell}^{\rm true})\rho_\ell^2-(1+\varepsilon_{T\ell}^{(*)})}{(1+\varepsilon_{T\ell}^{(*)})}.$$

In the fine-grained case, the amplitude adjusts until $1+\varepsilon_{T\ell}^{(n)}=(1+\varepsilon_{T\ell}^{\rm true})\rho_\ell^2$, so $\mathcal{F}_{BB}\to F_{BB}$ and the two power spectrum estimates and their error bars are the same. This form, though, takes longer to converge than the quadratic, and when the deviations are too large the iteration may not converge. (This is typical for the Newton-Raphson method.) A comparison of $\mathcal{F}_{BB}$ in Eq. (7.2) and v_B in Eq. (7.1) shows that, for wider bands, we can expect plus and minus fluctuations over the band which give $v_B=0$, but, because of the different weighting, will not give $\mathcal{F}_{BB}=F_{BB}$.

For the quadratic operator, another measure of the error bars is the variance of the Q_B, and this can partly take the non-Gaussian spread of the probability function for the quadratic into account. For the case considered here, this variance is diagonal in B. When the ensemble average is taken, the result is

$$\langle\Delta Q_B\Delta Q_B\rangle=F_{BB}^{-1}\frac{\sum_{\ell\in B}f_{B\ell}^{(q)}(1+\varepsilon_{T\ell}^{\rm true})^2/(1+\varepsilon_{T\ell}^{(*)})^2}{\sum_{\ell\in B}f_{B\ell}^{(q)}}$$
$$+\left[\frac{\sum_\ell f_{B\ell}^{(q)}(\varepsilon_{T\ell}^{\rm true}/\varepsilon_{T\ell}^{(*)}-1)}{\sum_\ell f_{B\ell}^{(q)}}\right]^2. \tag{7.3}$$

Thus in the limit that $\varepsilon_{T\ell}^{(*)}$ approaches $\varepsilon_{T\ell}^{\rm true}$, it reduces to F_{BB}^{-1}, the Fisher error we quote. However, the ρ_ℓ^2 corrections inherent in any realization preclude convergence to F_{BB}^{-1}, in such a way as to increase the error bars for low power modes and lowering them for high power modes over what F_{BB}^{-1} gives.

VIII. DISCUSSION

A. Computer resource demand

Evaluating the likelihood function is an $O(N^3)$ operation. Although both matrix inversion and determinant calculation are $O(N^3)$ operations, it is only the determinant evaluation that prevents the likelihood analysis from being $O(N^2)$. That is because only $C^{-1}\Delta$ is needed in the χ^2 evaluation, not the full inverse, and this can be potentially calculated via $O(N^2)$

iterative techniques. Today, a *single evaluation* of the likelihood function (and it must be evaluated many times to search the parameter space; see Appendix A) takes approximately 45 minutes for the $N=2928$ SK dataset on a DEC Alpha 250/ev5 and roughly a factor of five less on a Cray J90 parallel supercomputer; compressing to 1200 eigenmodes takes only five minutes on the DEC including overhead from the compression process. Upcoming balloon datasets are expected to have at least an order of magnitude more data—which translates to a factor of 1000 in execution time (and 100 in storage requirements). Megapixel datasets foreseen for upcoming satellite missions are clearly too large to analyze in this way with any foreseeable increase in computer speed.

The quadratic estimator is also $O(N^3)$ despite claims that it is $O(N^2)$ [7]. Finding good approximations that will reduce it to $O(N^2)$ is an unsolved problem, crucial for further study.

Even as we have implemented it, the quadratic is much faster than direct evaluation of the likelihood function. Starting from the signal-to-noise basis, one iteration of the quadratic estimator for the 10 SK bands of Section VI took 250 seconds to calculate the window function rotated into that basis, and 180 seconds to form the Fisher matrix and calculate the quadratic estimator on the Digital Equipment Corporation (DEC) Alpha, compressing to 1200 modes. The direct evaluation method, in contrast, requires a new rotation to the signal-to-noise basis at each band, which is roughly 5 minutes per band, using the same 1200-mode compression.

We have also performed the quadratic calculation via direct evaluation of δa_p and the Fisher matrix in the pixel basis, calculating quantities like $C^{-1}C_{T,p}$ using the Cholesky decomposition of C. This is somewhat faster than the same calculation in the eigenmode basis, although it does not allow easy implementation of signal-to-noise compression.

In Appendix A we explicitly calculate the Fisher matrix in $O(N^3)$ operations (the signal-to-noise eigenmode decomposition). To see what makes the quadratic estimator an $O(N^3)$ operation in general, it helps to rewrite it. If we define

$$y_p \equiv \Delta^T C^{-1} C_{T,p} C^{-1} \Delta \tag{8.1}$$

then $\langle y_p \rangle = \mathrm{Tr}(C^{-1}C_{T,p})$ and we can rewrite the quadratic estimator as

$$\delta a_p = \frac{1}{2} \sum_{p'} (F^{(a)})^{-1}_{pp'} (y_{p'} - \langle y_{p'} \rangle). \tag{8.2}$$

We can iteratively solve for the vector $C^{-1}\Delta$ and therefore y_p can be calculated. The slowest parts of the quadratic are the Fisher matrix and $\langle y_p \rangle$—both of which require calculating $C^{-1}C_{T,p}$.

If we can find a good approximation to $C^{-1}C_{T,p}$ that can be calculated in $O(N^2)$ operations, then the entire estimation procedure will be $O(N^2)$ for each element of the Fisher matrix. Since the Fisher matrix has N_p^2 elements, the estimation procedure is $O(N^2 N_p^2)$. If the number of parameters is roughly the square root of the number of pixels (as is expected to be the case for power spectrum estimation) then the estimation procedure is $O(N^3)$. For the largest maps, we can take advantage of the sparseness of the Fisher matrix to only calculate it in a band around the diagonal, reducing the process to $O(N^{2.5})$. {If we skip the power spectrum and go straight to the estimation of cosmological parameters, then $N_p \ll N$ and the process is $O(N^2)$. Of course, if C^{-1} is calculated directly [an $O(N^3)$ operation], then this is the most intensive step in calculating the Fisher matrix, and the whole process is still $O(N^3)$.}

The method we outline is completely general, allowing arbitrary chopping strategies and off-diagonal noise correlations, including those generated by the subtraction of constraints or foreground templates, as explained in Section II and Appendix A. We expect that these noise correlations will become increasingly important in future balloon and satellite experiments, which will exhibit both $1/f$ streaking and significant foreground contamination. Although we hope to find techniques that will reduce the computational load from $O(N^3)$ to $O(N^2)$, with general inhomogeneous noise this is a difficult problem. One approach is to try to find the best possible approximation to the generalized noise matrix which allows fast computation, then treat the residual perturbatively. Another is to rely on the special nature of the noise for a given experiment. For example, if an approximate set of eigenmodes along with their projection onto the spherical harmonics is known for the geometry and weighting of a particular dataset, then quantities like $C^{-1}C_{T,p}$ can be calculated without explicit inversion or matrix manipulation. Gorski's cut-sky spherical harmonics [25] have this property, but require an $O(N^3)$ Cholesky decomposition for their construction.

For mapping experiments, the parameter derivatives $C_{T,\ell}$ will be proportional to the Legendre polynomials, which can in turn be written as a sum over spherical harmonics using the appropriate summation formula. We have shown that at high ℓ, two-dimensional (flat-sky) fourier modes with wave number $|\mathbf{Q}| \sim \ell$ are very useful, and expect that they will be effective as we look for ways to improve the computational speed. For COBE DMR, using an approximate weight is adequate for some statistical measures, but for high precision work the residual 60° correlation and constraints should be taken into account. For upcoming balloon and satellite experiments, full and correct modelling of the noise and its behavior in various subspaces will be essential for achieving the forecasted accuracy [2,3] in cosmological parameter determinations.

B. Redshift surveys

So far, we have concentrated our analysis on applications to CMB anisotropy data. However, much of it can be carried over to estimate the power spectrum of other sorts of data, particularly that of upcoming redshift surveys [38,19]. In that case, we partition the three-dimensional volume probed by the surveys into bins $i=1,\ldots,N$ and use counts-in-cells as the data $\Delta_i = s_i + n_i$. Now, the ''beam function'' becomes the selection function of the survey restricted to the individual bins, which accounts for the flux cutoff in its observational bands. The noise becomes considerably more complicated: it is the ''shot noise'' which comes from the sampling of the underlying density field in whose correlations we are actually interested. This noise is not Gaussian, but Poissonian (and only that if we ignore correlations within

the bin); to use this formalism requires that we have enough galaxies per bin that a Gaussian approximation is adequate, but small enough that the correlations within the bin are ignorable (and small enough that we still have information on scales of interest). In that case, the Poisson noise term has $\langle n_i^2 \rangle$ given by the counts in the bin. Of course, there are further complications due to redshift-space distortions. For an alternative to this procedure, see [39].

C. Summary

We have demonstrated two techniques for determining the power spectrum of CMB fluctuations from realistic microwave data. We have presented an analysis of both a direct likelihood search and a specific quadratic estimator; the most important result of this paper is the proof that the iterated application of the quadratic estimator is a fast method for finding the peak and curvature of the likelihood function.

Our methods easily incorporate such realistic features as convoluted chopping strategies, incomplete sky coverage, and the removal of linear constraints from the data. As implemented today, our method requires $O(N^3)$ operations in order to deal with these complications. We have applied the techniques to both the DMR and SK datasets, which exhibit all of these complications. Numerically, our results agree quite well with other analyses of these datasets.

We have also discussed several caveats in the further use of the power spectrum, associated with the non-Gaussian nature of the posterior distribution of the $\mathcal{C}_\ell$. This can have repercussions in any analysis (such as χ^2, or even in our own rebinning techniques) which implicitly or explicitly assume Gaussianity of the distribution (*i.e.*, the constant curvature of the log-likelihood).

The traditional procedure for reporting constraints on the power spectrum is the band-power method, where the power spectrum estimate is considered to be a measurement of the power averaged through some specific filter. In the past this filter has been given by the trace of the window function, W_ℓ. We advocate a generalization of this procedure where the filter is derived from the Fisher matrix instead. With this better definition of the filter, the new technique will improve the accuracy of analyses that start from band-power estimates.

D. Quadratic estimation cookbook

We now summarize the complete algorithm for quadratic power spectrum estimation:

(1) Obtain the data and the error or weight matrix C_N (including the effects of constraints as discussed in Appendix A).

(2) Choose an initial ℓ binning, as discussed in Section IV.

(3) Calculate the window function matrix $W_{pp'}(\ell)$, Eq. (2.8), perhaps averaged over the ℓ bins.

(4) Choose a power spectrum $\mathcal{C}_\ell^{(0)}$ to begin the iteration.

(5) Calculate C_T for $\mathcal{C}_\ell^{(i)}$ ($i=0$ for the first iteration), from Eq. (2.7).

(6) If desired, the rest of the calculation can be performed in the signal-to-noise basis of Appendix A. In that case, C_T and the data are transformed according to Eqs. (A4)–(A5).

(7) Calculate the parameter derivatives $C_{T,B} \equiv \partial C_T / \partial q_B$ in each band, using Eqs. (2.19)–(2.20) or, in the S/N basis, Eqs. (A7)–(A8). The parameter q_B, Eq. (4.10), is the fractional difference from $\mathcal{C}_\ell^{(i)}$.

(8) Calculate the Fisher Matrix, Eq. (2.17) or Eq. (A10), for the chosen bands.

(9) Calculate the complete quadratic δq_B using Eq. (2.18) or Eq. (A11), and set

$$\mathcal{C}_\ell^{(i+1)} = \sum_B (1+\delta q_B)\mathcal{C}_\ell^{(i)} \chi_B(\ell).$$

(10) Lather, rinse, and repeat with Step 5 until $\delta q_B \approx 0$ to the desired accuracy.

This description has not included the complications associated with rebinning (see Section IV) and the use of filter functions for reporting bandpowers (see Section VI).

E. Numerical results

Our power spectrum estimates for COBE DMR and SK are available over the WWW and by anonymous FTP in the directory **file://ftp.cita.utoronto.ca/cita/knox/pspec_Cl/**. These numerical results include the results of both the full-likelihood and quadratic procedures; for the latter we include the results for ''orthogonalized'' and ''shaped'' bands, along with appropriately tabulated filter functions.

ACKNOWLEDGMENTS

The authors thank Scott Dodelson, Andrew Hamilton, Uros Seljak and Max Tegmark for useful conversations, and Ted Bunn and Kris Gorski for providing the results of their analyses. A.J. and L.K. would especially like to acknowledge the hospitality of the Aspen Center for Physics, where portions of this work were completed. Some of the computations described herein were performed by A.J. on the computers of the National Energy Research Scientific Computing Center (NERSC).

APPENDIX A: SIGNAL-TO-NOISE EIGENMODES AND CONSTRAINTS

Some of the calculations described in this paper are performed in the ''signal-to-noise eigenmode'' basis [13,15–17]. To effect this transformation, we model the observation at a pixel as

$$\Delta_i = s_i + n_i \tag{A1}$$

where s_i is the contribution to the signal, and n_i to the noise. They have zero means, and independent correlation matrixes $\langle n_i n_{i'} \rangle = C_{nii'}$ and $\langle s_i s_{i'} \rangle = \sigma_{\rm th}^2 C_{Tii'}$. Here, $\sigma_{\rm th}$ is the unknown amplitude of the signal to be measured (along with other possible parameters in C_T).

We may ascribe more than the experimental noise contribution to n_i: in particular, any contributions to the observation with which we are not concerned in a given part of the calculation can be included in the noise. This could be the CMB monopole and dipole, or constraints such as averages and gradients that may have been removed from the data to compensate for atmospheric and instrumental drift. For

COBE DMR, we allow arbitrary amplitudes for the monopole (one component) and the dipole (three components); for SK, we allow an arbitrary average for each ''demodulation'' [11], giving a total of 66 separate amplitudes. In the event, each constraint component c can be represented by a template in pixel space, Υ_{ci}, with an unknown amplitude, κ_c. Thus, the CMB signal plus experimental noise is given by the combination $\Delta_i - \Sigma_c \kappa_c \Upsilon_{ci}$, which is distributed as a Gaussian with correlation matrix $C_n + \sigma_{\rm th}^2 C_T$. We do not know the amplitudes κ_c *a priori*, but we can assign them a prior probability distribution given by a zero-mean Gaussian with very large variances in the matrix $\langle \kappa_c \kappa_{c'} \rangle = K_{cc'}$, (compared to the expected signal and the experimental noise), and then marginalize over the amplitudes κ_c. It turns out that this marginalization procedure can be done analytically, and the result is that the likelihood is now given by a zero-mean Gaussian distribution in Δ alone, with a full correlation matrix including a new term accounting for the unknown constraints:

$$\langle \Delta_i \Delta_{i'} \rangle = \sigma_{\rm th}^2 C_{Tii'} + C_{nii'} + C_{Cii'} \tag{A2}$$

where

$$C_{Cii'} = \sum_{cc'} \Upsilon_{ci} K_{cc'} \Upsilon_{c'i'} \tag{A3}$$

is the constraint or template correlation matrix. For a diagonal matrix of priors, $K = \mathrm{diag}(\sigma_c^2)$, this reduces to $C_{Cii'} = \Sigma_c \sigma_c^2 \Upsilon_{ci} \Upsilon_{ci'}$.

In effect, we have added a new term to the noise correlation, $C_N = C_n + C_C$; in the following we shall implicitly include this in C_N. In the limit $\sigma_c^2 \to \infty$, this procedure is equivalent to projecting out the constrained components from the data and the correlation matrix; because this projection results in a singular matrix, the marginalization procedure is numerically simpler (but see [19] for the details of an implementation of the projection procedure). Note also that this procedure is more generally useful: in particular it provides a new technique for removing foreground contamination with a known spatial morphology [40].

With this split of the observation into signal and (generalized) noise, we first perform a so-called whitening transformation

$$\begin{aligned} C_N &\to C_N^{-1/2} C_N C_N^{-1/2} = I; \\ C_T &\to C_N^{-1/2} C_T C_N^{-1/2}; \\ \Delta &\to C_N^{-1/2} \Delta. \end{aligned} \tag{A4}$$

Here, $C_N^{-1/2}$ is the inverse of the Cholesky decomposition of C_N or its Hermitian Square Root. Now, the noise part of the ''new data,'' $C_N^{-1/2}\Delta$, are uncorrelated, with unit variance. We next diagonalize the signal matrix with its matrix of eigenvectors,

$$\begin{aligned} C_T &\to R^\dagger C_N^{-1/2} C_T C_N^{-1/2} R = \mathcal{E} = \mathrm{diag}(\mathcal{E}_k); \\ \Delta &\to R^\dagger C_N^{-1/2} \Delta = \xi. \end{aligned} \tag{A5}$$

In this new basis, the data ξ_k are uncorrelated with variance $\langle \xi_k^2 \rangle = 1 + \sigma_{\rm th}^2 \mathcal{E}_k$. The $\mathcal{E}_k$ are ''eigenmodes of signal-to-noise''; modes with large eigenvalue are expected to be well-measured (for the specific theory matrix C_T used in the transformation); modes with small eigenvalue are poorly measured (and do not contribute significantly to the likelihood). In particular, we use this transformation to compress the SK data: we pick a fiducial model (in this case, $n_s = 1.45$ tilted standard CDM, which fits the SK data alone reasonably well) and calculate the modes for this theory. We then discard all but the top 1200 modes (of 2928 data points) and treat this linear combination as our new dataset (for which we subsequently calculate all likelihoods without further approximation); elsewhere [13] we show that this truncation to 1200 theory-dependent modes is an excellent approximation to the entire dataset.

Note that in the S/N basis, the likelihood as a function of the amplitude $\sigma_{\rm th}$ is quite easy to compute for arbitrary values:

$$-2 \ln P(\Delta | \sigma_{\rm th}^2 C_\ell) = \sum_k \left(\ln(1 + \sigma_{\rm th}^2 \mathcal{E}_k) + \frac{\xi_k^2}{1 + \sigma_{\rm th}^2 \mathcal{E}_k} \right) \tag{A6}$$

(up to a constant). In the calculation of the likelihood as a function of the values of the power spectrum, we iterate by ascribing only the single C_ℓ (or within a band, with some shape for C_ℓ over the band) of interest to the signal, s_i, and the rest to the noise, n_i, along with the actual experimental noise, and any terms due to constraints such as dipole removal. This way, the single parameter of interest at anytime is just the amplitude $\sigma_{\rm th}^2 \propto \mathcal{C}_\ell$ for that band, for which the likelihood is easy to compute once the S/N mode decomposition has been determined.

We also compute the quadratic C_ℓ estimators in this basis. First, we define the window function matrix [Eq. (2.8)] transformed into this basis,

$$G_{kk'}(\ell) = \sum_{ii'} (R^\dagger C_N^{-1/2})_{ki} W_{ii'}(\ell) (C_N^{-1/2} R)_{i'k'}. \tag{A7}$$

This quantity comes into the calculations because it is related to the derivative of the theory covariance in the eigenbasis,

$$\begin{aligned} \mathcal{E}_{kk',\ell} &\equiv \sum_{ii'} (R^\dagger C_N^{-1/2})_{ki} \frac{\partial C_{Tii'}}{\partial \mathcal{C}_\ell} (C_N^{-1/2} R)_{i'k'} \\ &= \frac{\ell + 1/2}{\ell(\ell+1)} G_{kk'}(\ell). \end{aligned} \tag{A8}$$

Here we have assumed that we are interested in the individual $\mathcal{C}_\ell$ values. If we are instead interested in the values over some bands, B, of ℓ with some assumed spectral shape $\mathcal{C}_\ell^{\rm shape}$, then we use instead

$$\mathcal{E}_{kk',B} = \sum_{\ell \in B} \mathcal{E}_{kk',\ell} \mathcal{C}_\ell^{\rm shape}. \tag{A9}$$

Note that, unlike the full theory covariance, $\mathcal{E} = \mathrm{diag}(\mathcal{E}_k)$, these derivatives have off-diagonal components. In Eqs.

(A10) and (A11) below, $\mathcal{E}_{kk',B}$ and $\mathcal{E}_{kk',\ell}$ can be used interchangeably, depending on whether one is estimating individual $\mathcal{C}_\ell$ values, or those in bands.

The Fisher matrix for the parameters $\mathcal{C}_\ell$ [Eq. (2.17)] then becomes

$$F_{\ell\ell'}=\sum_{kk'}\frac{\mathcal{E}_{kk',\ell}\mathcal{E}_{k'k,\ell'}}{(1+\sigma_{\rm th}^2\mathcal{E}_k)(1+\sigma_{\rm th}^2\mathcal{E}_{k'})}. \tag{A10}$$

Then the full quadratic estimator [compare Eq. (2.18)] is

$$\delta\mathcal{C}_\ell=\frac{1}{2}\sum_{\ell'}F^{-1}_{\ell\ell'}\left(\sum_{kk'}\frac{\xi_k\mathcal{E}_{kk',\ell'}\xi_{k'}}{(1+\sigma_{\rm th}^2\mathcal{E}_k)(1+\sigma_{\rm th}^2\mathcal{E}_{k'})}-\sum_k\frac{\mathcal{E}_{kk,\ell'}}{1+\sigma_{\rm th}^2\mathcal{E}_k}\right). \tag{A11}$$

Note that in this formalism the $O(N^3)$ transformation into the S/N basis is the most expensive part of the calculation; the remainder requires trivial $O(N^2)$ sums and the inverse of the (comparitively small) $N_p\times N_p$ Fisher matrix.

APPENDIX B: REBINNING ORTHOGONAL LINEAR COMBINATIONS

Here we derive Eq. (6.4) which tells how to rebin orthogonal linear combinations of $\mathcal{C}_\ell$. We then generalize to the case where the initial binning is coarser than $\Delta\ell=1$.

We start by parameterizing the spectrum as

$$\mathcal{C}_\ell=q_\ell\mathcal{C}_\ell^{\rm shape} \tag{B1}$$

and then transforming the q_ℓ to $\tilde{q}=Z^Tq$. If we assume the shape is correct, then the expectation value of $\tilde{q}^N_\lambda\equiv\tilde{q}_\lambda/N_\lambda$ is independent of λ, where $N_\lambda=\Sigma_\ell Z_{\ell\lambda}$. Since we always want to average things together that we expect to be measurements of the same quantity, we average together the $\tilde{q}^N_\lambda$. Calling the result $\tilde{q}^N_\beta$:

$$\tilde{q}^N_\beta=\frac{\sum_{\lambda\lambda'}\tilde{q}^N_\lambda F^{\tilde{q}^N}_{\lambda\lambda'}}{\sum_{\lambda\lambda'}F^{\tilde{q}^N}_{\lambda\lambda'}}. \tag{B2}$$

Here, and in the following, the sums over λ and λ' extend only over the range determined by β. For example, if for $\beta=1$ we are averaging together the first three linear combinations, then the sums over λ and λ' run from one to three.

Using the fact that $F^{\tilde{q}^N}_{\lambda\lambda'}=N_\lambda F^{\tilde{q}}_{\lambda\lambda'}N_{\lambda'}$ and specializing to the case where $F^{\tilde{q}}_{\lambda\lambda'}=\delta_{\lambda\lambda'}$ (which is the case for $Z=L$ or $Z=F^{1/2}$) we get

$$\tilde{q}^N_\beta=\frac{\Sigma_\lambda\tilde{q}_\lambda N_\lambda}{\Sigma_\lambda N_\lambda^2}. \tag{B3}$$

Plugging in $\tilde{q}_\lambda=Z_{\ell\lambda}\mathcal{C}_\ell/\mathcal{C}_\ell^{\rm shape}$ and $N_\lambda=\Sigma_\ell Z_{\ell\lambda}$ a little algebra shows that the filter function is

$$f^{(\mathcal{C})}_{\beta\ell}=\sum_\lambda f^{(\mathcal{C})}_{\lambda\ell}N_\lambda \tag{B4}$$

where

$$f^{(\mathcal{C})}_{\lambda\ell}=Z_{\ell\lambda}/\mathcal{C}_\ell^{\rm shape} \tag{B5}$$

is the filter function prior to rebinning. Therefore

$$\mathcal{C}_\beta=\frac{\sum_\lambda\tilde{q}_\lambda N_\lambda}{\sum_\ell f^{(\mathcal{C})}_{\beta\ell}}=\frac{\sum_\ell q_\ell\mathcal{C}_\ell^{\rm shape}f^{(\mathcal{C})}_{\beta\ell}}{\sum_\ell f^{(\mathcal{C})}_{\beta\ell}} \tag{B6}$$

which is Eq. (6.4).

As an aside, we consider the case of rebinning all the estimates into one bin. We expect that the estimated power and filter function in this case should be independent of the basis of the original estimates; they should not depend on Z. Indeed, this is the case:

$$\tilde{q}^N_\beta=\frac{\sum_{\ell\ell'\lambda}\mathcal{C}_\ell/\mathcal{C}_\ell^{\rm shape}Z_{\ell\lambda}Z_{\ell'\lambda}}{\sum_{\ell\ell'\lambda}Z_{\ell\lambda}Z_{\ell'\lambda}}=\frac{\sum_{\ell\ell'}\mathcal{C}_\ell/\mathcal{C}_\ell^{\rm shape}F^q_{\ell\ell'}}{\sum_{\ell\ell'}F^q_{\ell\ell'}}. \tag{B7}$$

The second equality follows since when the sum over λ goes over all λ, $Z_{\ell\lambda}Z^T_{\lambda\ell'}=F^q_{\ell\ell'}$.

When the initial binning is coarser than $\Delta\ell=1$, then this procedure is slightly more complicated. We introduce the sub-band structure filter, $f^{(\mathcal{C})}_{B\ell}$, which is defined within each band B. The sub-band structure is given by

$$f^{(\mathcal{C})}_{B\ell}=\sum_{\ell'}F^{(\mathcal{C})}_{\ell\ell'}\mathcal{C}^{\rm shape}_{\ell'} \tag{B8}$$

which is the same as Eq. (4.6). The difference here is that we have not calculated $F^{(\mathcal{C})}_{\ell\ell'}$ and thus must rely on analytic knowledge of it.

The rebinning procedure is the same for the $\Delta\ell=1$ initial binning except

$$\mathcal{C}_\ell^{\rm shape}\to\mathcal{C}_B^{\rm shape}=\frac{\sum_{\ell\in B}f^{(\mathcal{C})}_{B\ell}\mathcal{C}_\ell^{\rm shape}}{\sum_{\ell\in B}f^{(\mathcal{C})}_{B\ell}}, \tag{B9}$$

$$N_\lambda\to N_\beta=\sum_B Z_{B\beta} \tag{B10}$$

and

$$f^{(\mathcal{C})}_{\beta\ell} \to f^{(\mathcal{C})}_{\beta'\ell} = \left(\frac{f^{(\mathcal{C})}_{B\ell}}{\sum_{\ell \in B} f^{(\mathcal{C})}_{B\ell}} \right) f^{(\mathcal{C})}_{\beta' B(\ell)} \tag{B11}$$

where

$$f^{(\mathcal{C})}_{\beta' B} = \sum_{\beta \in \beta'} \frac{Z_{B\beta}}{\mathcal{C}^{\rm shape}_B} N_\beta . \tag{B12}$$

The final result is

$$\mathcal{C}_{\beta'} = \frac{\sum_\ell q_{B(\ell)} \mathcal{C}^{\rm shape}_\ell f^{(\mathcal{C})}_{\beta'\ell}}{\sum_\ell f^{(\mathcal{C})}_{\beta'\ell}} = \sum_B X_{\beta' B} q_B . \tag{B13}$$

The last equality is used to define the matrix $X_{\beta' B}$ and to emphasize that $\mathcal{C}_{\beta'}$ is simply a linear transformation of the original q_B parameters. The Fisher matrix for $\mathcal{C}_{\beta'}$ can easily be calculated from that for q_B, using the general rule for how the Fisher matrix changes under linear transformation of the parameters.

[1] L. Knox, Phys. Rev. D **52**, 4307 (1995).

[2] G. Jungman, M. Kamionkowski, A. Kosowsky, and D.N. Spergel, Phys. Rev. Lett. **76**, 1007 (1996); Phys. Rev. D **54**, 1332 (1995): M. Zaldarriaga, D. Spergel, and U. Seliak, astro-ph/9702157.

[3] J.R. Bond, G. Efstathiou, and M. Tegmark, astro-ph/9702100.

[4] A.H. Jaffe, L. Knox, and J.R. Bond (in preparation).

[5] A.H. Jaffe, L. Knox, and J.R. Bond, Proceedings of the Eighteenth Texas Symposium on Relativistic Astrophysics, Chicago, IL, 1996, edited by A. Olinto, J. Frieman, and D. Schramm (World Scienfitic, Singapore, in press).

[6] M.G. Hauser and P.J.E. Peebles, Astrophys. J. **185**, 757 (1973); E.L. Wright, *ibid.* **436**, 443 (1994).

[7] M. Tegmark, Phys. Rev. D **55**, 5895 (1997).

[8] L. Knox, J.R. Bond and A. Jaffe, in [5].

[9] C.L. Bennett, A.J. Banday, K.M. Gorski, G. Hinshaw, P.D. Jackson, P. Keegstra, A. Kogut, G.F. Smoot, D. Wilkinson and E.L. Wright, Astrophys. J. Lett. **464**, L1 (1996), and 4-year DMR references therein.

[10] A. Kogut, A.J. Banday, C.L. Bennett, K.M. Gorski, G. Hinshaw, G.F. Smoot and E.L. Wright, Astrophys. J. Lett. **464**, L5 (1996); A. Kogut, A.J. Banday, C.L. Bennett, K.M. Gorski, G. Hinshaw, P.D. Jackson, P. Keegstra, L. Lineweaver, G.F. Smoot, T. Tenorio and E.L. Wright, Astrophys. J. **470**, 653 (1996); A.J. Banday, K.M. Gorski, C.L. Bennett, G. Hinshaw, A. Kogut and G.F. Smoot, Astrophys. J. Lett. **468**, L85 (1996).

[11] C.B. Netterfield, M.J. Devlin, N. Jarosik, L. Page and E.J. Wollack, Astrophys. J. **474**, 47 (1997): E.J. Wollack, M.J. Devlin, N. Jarosik, C.B. Netterfield, L. Page and D. Wilkinson, *ibid.* **476**, 440 (1997).

[12] C. Lineweaver and D. Barbosa, astro-ph/9706077.

[13] J.R. Bond and A. Jaffe, report, in *Proceedings of the XVIth Moriond meeting, ''Microwave Background Anisotropies,''* edited by F.R. Bouchet *et al.* (Editions Frontières, Gif-Sur-Yvette, France, 1997).

[14] S. Hancock and G. Rocha, astro-ph/9612016; in [13].

[15] J.R. Bond, Astrophys. Lett. Commun. **32**, 63 (1995).

[16] J.R. Bond, Phys. Rev. Lett. **74**, 4369 (1995).

[17] E.F. Bunn and M. White, Astrophys. J. **480**, 6 (1997).

[18] For a review of signal-to-noise eigenmodes, see M. Tegmark, A.M. Taylor and A.F. Heavens, Astrophys. J. **480**, 22 (1997).

[19] M. Tegmark, A.J.S. Hamilton, M.A. Strauss, M.S. Vogeley and A.S. Szalay, astro-ph/9708020.

[20] M. Tegmark, Mon. Not. R. Astron. Soc. **280**, 299 (1995); Phys. Rev. D **56**, 4514 (1997).

[21] W.H. Press, B. Flannery, S.A. Teukolsky and W.T. Vetterling, *Numerical Recipes in Fortran*, 2nd ed. (Cambridge University Press, Cambridge, England, 1992).

[22] A.J.S. Hamilton, astro-ph/9701008; astro-ph/9701009.

[23] M. Tegmark and A. Hamilton, in [5].

[24] S.P. Boughn, E.S. Cheng, D.A. Cottingham, and D.J. Fixsen, Astrophys. J. Lett. **391**, L49 (1992).

[25] K.M. Gorski, Astrophys. J. Lett. **430**, L85 (1994); K.M. Gorski, A.J. Banday, C.L. Bennett, G. Hinshaw, A. Kogut, G.F. Smoot and E.L. Wright, *ibid.* **464**, L11 (1996); K.M. Gorski, astro-ph/9701191.

[26] C. Lineweaver and G. Smoot, COBE note 5051 (1993).

[27] R. Kneissl and G. Smoot, COBE note 5053 (1993).

[28] E. Leitch (private communication).

[29] C.B. Netterfield and L. Page (private communication).

[30] J.R. Bond, in *Cosmology and Large Scale Structure*, Les Houches Session LX, 1993, edited by R. Schaeffer *et al.* (Elsevier Science, Amsterdam, 1996), pp. 469–674.

[31] A map of the North Celestial Pole region has been made by Wiener-filtering the SK data: M. Tegmark, A. de Oliveira-Costa, M.J. Devlin, C.B. Netterfield, P. Page and E.J. Wollack, Astrophys. J. Lett. **474**, L77 (1997); See also [40].

[32] C. Bennett *et al.*, MAP experiment home page, http://map.gsfc.nasa.gov (1996).

[33] M. Bersanelli *et al.*, *COBRAS/SAMBA, The Phase A Study for an ESA M3 Mission*, report (1996); Planck home page, http://astro.estec.esa.nl/SA-general/Projects/Cobras/cobras.html (1996).

[34] E. Cheng *et al.*, TopHat home page, http://cobi.gsfc.nasa.gov/msam-tophat.html (1997).

[35] P. Richards *et al.*, MAXIMA home page, http://physics7.berkeley.edu/group/cmb/gen.html (1997).

[36] A. Lange *et al.*, Boomerang home page, http://astro.caltech.edu/~mc/boom/boom.html (1997).

[37] P. Lubin *et al.*, ACE/Beast home page, http://www.deepspace.ucsb.edu/research/Sphome.html (1997).

[38] J.E. Gunn and D.H. Weinberg, in *Wide-Field Spectroscopy and the Distant Universe*, edited by S.J. Maddox and A. Aragòn-Salamanca (Singapore, World Scientific, 1995), p. 3; M. Tegmark, Phys. Rev. Lett. **79**, 3806 (1997).

[39] S. Dodelson, L. Hui and A.H. Jaffe (in preparation).

[40] A.H. Jaffe, D. Finkbeiner and J.R. Bond (in preparation).